SEDIMENTOLOGY the journal of the International Association of Sedimentologists IAS

Sedimentology (2024) **71**, 1084–1112 doi: 10.1111/sed.13168

Large-scale sedimentary shift induced by a mega-dam in deltaic flats

JIE WANG*,†, ZHIJUN DAI*,‡, SERGIO FAGHERAZZI§, YAYING LOU¶, XUEFEI MEI* and BINBIN MA*

**State Key Laboratory of Estuarine and Coastal Research, East China Normal University, Shanghai 200241, China (E-mail: zjdai@sklec.ecnu.edu.cn) (E-mail: xfmei@geo.ecnu.edu.cn)*

†Department of Physical Geography, Faculty of Geosciences, Utrecht University, Utrecht 3584, The Netherlands

‡Laboratory for Marine Geology, Qingdao National Laboratory for Marine Science and Technology, Qingdao 266237, China

§Department of Earth and Environment, Boston University, Boston, MA 02215, USA

¶Zhuhai-MUST Science and Technology Research Institute, Zhuhai 519099, China

Associate Editor – J.P. Walsh

ABSTRACT

Deltas are crucial for land building and ecological services due to their ability to store mineral sediment, carbon and potential pollutants. A decline in suspended sediment discharge in large rivers caused by the construction of mega-dams might imperil deltaic flats and wetlands. However, there has not been clear evidence of a sedimentary shift in the downstream tidal flats that feed coastal wetlands and the intertidal zone with sediments. Here, integrated intertidal/subaqueous sediment samples, multi-year bathymetries, fluvial and deltaic hydrological and sediment transport data in the Nanhui tidal flats and Nanhui Shoal in the Changjiang (Yangtze) Delta, one of the largest mega-deltas in the world, were analysed to discern how sedimentary environments changed in response to the operations of the Three Gorges Dam. Results reveal that the coarser sediment fractions of surficial sediments in the subaqueous Nanhui Shoal increased between 2004 to 2021, and the overall grain size coarsened from 18.5 to 27.3 μm. Moreover, intertidal sediments in cores coarsened by 25% after the 1990s. During that period, the northern part of the Nanhui Shoal suffered large-scale erosion, while the southern part accreted in recent decades. Reduced suspended sediment discharge of the Changjiang River combined with local resuspension of fine-grained sediments are responsible for tidal flat erosion. This study found that the spatial pattern of grain-size parameters has shifted from crossing the bathymetric isobaths to being parallel to them. Higher tide level and tidal range induced by sea-level rise, an upstream increase in bed shear stress and larger waves likely further exacerbated erosion and sediment coarsening in deltaic flats. As a result, this sediment-starved estuary coupled with sea-level rise and artificial reclamations have enhanced the vulnerability of tidal flats in Changjiang Delta, this research is informative to the sedimentary shift of worldwide mega-deltas.

Keywords Anthropogenic stress, Changjiang (Yangtze) Delta, deltaic flats, hydro-morphodynamics, sedimentary shift.

INTRODUCTION

Deltaic tidal flats are found in mega-deltas as a result of riverine inputs and marine processes, and provide crucial bio-ecological services such as storm defence, organic carbon sequestration and wildlife habitat (Möller *et al.*, 2014; Rogers *et al.*, 2019; Fagherazzi *et al.*, 2020). The stability and vulnerability of deltaic flats are primarily regulated by mineral sediment availability and estuarine hydrodynamics (Kirwan & Megonigal, 2013; Ganju *et al.*, 2015; Donatelli *et al.*, 2020).

Globally, 86% of the total terrigenous sediment is delivered into the oceans by rivers. Global annual sediment discharge reached 2.3×10^{10} t during the last century; this sediment fed deltaic flats and subaqueous areas near tidal wetlands and intertidal zones (Milliman & Meade, 1983; Tamura *et al.*, 2012). In general, the seaward dispersal patterns of fluvial sediments in estuaries and deltas are regulated by the total amount of inputs, hydrodynamics (tides, waves, etc.) and subaqueous topographic features (Walsh & Nittrouer, 2009). However, the fluvial discharge and sediment supply have been severely reduced over the past several decades because of upstream damming, leading to the degradation and instability of deltaic flats (Nilsson *et al.*, 2005; Blum & Roberts, 2009; Syvitski *et al.*, 2009; Dai *et al.*, 2018). Threatened by land subsidence, erosion, accelerating sea-level rise and human disturbances, the large-scale wetlands and tidal flats in mega-deltas are now more vulnerable, also because the delivery patterns and budgets of sediment input from upstream rivers to the adjacent coasts and delta front have been modified (Syvitski *et al.*, 2009; Thorne *et al.*, 2018). For instance, in the Mississippi, Nile, Yellow (Huanghe) and Mekong deltas, the loss of tidal flats and shoreline retreat were triggered by insufficient riverine sediment inputs (Paola *et al.*, 2011; Marriner *et al.*, 2012; Wang *et al.*, 2017; Kondolf *et al.*, 2022). If there is enough sediment for tidal flat accretion or enough space for landward transgression, their deterioration can be alleviated during sea-level rise (Kirwan *et al.*, 2016; Schuerch *et al.*, 2018).

Increasingly frequent and extensive anthropogenic activities (such as reclamation, aquaculture and port construction) have led to the permanent disappearance of many intertidal areas (Kennish, 2001; Hong *et al.*, 2010; Murray *et al.*, 2019, 2022). However, there are still knowledge gaps and higher-resolution analyses are needed to demonstrate whether human activities have triggered a change in the bottom sediments of tidal flats and deltaic wetlands, especially in deltas that have historically been sediment-rich (Chambers *et al.*, 1999; Schile *et al.*, 2014; Rodriguez *et al.*, 2020; Wang *et al.*, 2022a). Sediment grain-size parameters are important indicators for examining variations in hydrodynamic–sedimentary environments in mega-deltas (Imperato *et al.*, 1988; Hori *et al.*, 2002; Bianchi & Allison, 2009). The total available amount, transport pattern and grain size of fluvial/marine sediments interact with hydrodynamics to regulate the sedimentary processes and geomorphology in deltaic shoals (Orton & Reading, 1993). Studies have shown that sediment coarsening in tidal flats and wetlands reduces the carrying capacity of biogenic elements, microorganisms and pollutants, weakening the overall functions of pollutant degradation, organic matter accumulation and biodiversity (Canuel *et al.*, 2007; Burdon *et al.*, 2013; Bainbridge *et al.*, 2018). On the contrary, the deposition of fine sediment can promote blue carbon storage and provide habitats for benthic fauna (Widdows & Brinsley, 2002; Lee *et al.*, 2019).

Current studies have focused on the gain and loss of tidal wetlands and flats, concentrating on elevation variations at limited subaerial sites. A sedimentary shift across deltaic tidal flats will likely trigger a vegetation change, endangering the long-term delta survival (Kirwan & Megonigal, 2013; Tessler *et al.*, 2015). Due to the scarcity of integrated data on hydrodynamics, bathymetry, and intertidal and subtidal sediments, sedimentary shifts in tidal flats in mega-deltas are not fully understood.

The overall growth rate of tidal flats in the Changjiang (Yangtze) Delta declined from about 12 km^2/year in the 1970s to 3.3 km^2/year in 1998. The tidal flats were further degraded, and the subaqueous delta experienced severe erosion, due to reduced sediment supply after the construction of a series of dams in the river watershed [including the largest one in the series; the Three Gorges Dam (TGD)] (Yang *et al.*, 2005). Chen *et al.* (2016) through satellite monitoring found that salt marshes and mudflats in the Changjiang Delta have decreased by 38% and 31%, respectively, during the past three decades. In addition, Ge *et al.* (2015) suggested that sea-level rise and reduced sediment supply promoted the encroachment of invasive species and reduction of native species in the eastern Chongming Island, Changjiang Delta, thus affecting primary productivity

and intertidal vegetation patterns. Cui *et al.* (2015) determined with the SPRC (Source–Pathway–Receptor–Consequence) model that the proportion of deltaic wetlands with high vulnerability will increase by 6.9% by 2100, under a sea-level rise of 0.59 cm/year [Intergovernmental Panel on Climate Change's (IPCC)–An emphasis on fossil fuels (A1F1) scenario]. Dai *et al.* (2014, 2018) indicated that the depocentres in deltaic distributaries and submerged areas of the Changjiang Delta shifted between 1958 and 2009. These depocentres regulate the equilibrium of the sedimentary–morphodynamic system. Moreover, sustained accretion and progradation of salt marshes and tidal flats were confirmed on the East Chongming Shoal (Yang *et al.*, 2020; Leonardi *et al.*, 2021). Therefore, whether deltaic tidal flats will gain or lose area in the future is still unknown, and there is a need to elucidate the spatial–temporal transfers of sediments in the system.

The Nanhui Shoal, with an area of 130 km^2, is the largest and fastest accreting marginal tidal shoal and wetlands in the Changjiang Delta (Fig. 1A and B). The adjacent Nanhui tidal flats with elevations between 0 m and −2 m exceed 200 km^2 in area and provide valuable habitats for organisms. Thus, the sedimentary and geomorphic trajectories of these two systems can reflect changes in sediment inputs and marine hydrodynamics at multiple spatial and temporal scales.

The main objectives of the study are to: (i) examine the spatial changes of sedimentary environments in the Nanhui Shoal and nearby intertidal flats in the last two decades; (ii) discern the bathymetric erosion and deposition patterns; and (iii) diagnose potential risks to morphodynamic sustainability caused by a sedimentary shift around the Nanhui Shoal and marginal tidal flats. Insights will help to improve understanding of the sedimentary response of tidal flats to anthropogenic and climatic stressors in mega-deltas.

STUDY SITE

The Changjiang River originates from the Qinghai–Tibet Plateau and flows eastward into the East China Sea. In the catchment, the runoff and sediment-yielding processes are influenced by the East Asian monsoon (Fig. 1A) (Dai & Liu, 2013). Over the past two millennia, the Changjiang Delta evolved a funnel-shaped configuration with four subaqueous distributaries, and the south flank prograded south-eastward with an average rate of 25 m/year (Fig. 1B) (Chen *et al.*, 1988; Hori *et al.*, 2001; Fan *et al.*, 2017). Mean annual water discharge and suspended sediment discharge were 9.05×10^{11} m^3 and 4.33×10^8 t at Datong station during the period 1950 to 2000 (Dai *et al.*, 2016a). Between 2003 and 2020, the suspended sediment discharge sharply dropped by over 70% (to 1.19×10^8 t) after the construction of the TGD, while the water discharge remained stable (9.10×10^{11} m^3) (Dai *et al.*, 2018; CWRC, 2020). Four marginal tidal wetlands are distributed in the Changjiang Delta: East-Chongming Shoal, East-Hengsha Shoal, Jiuduansha Shoal and Nanhui Shoal (Fig. 1B) (Chen *et al.*, 1999). The total intertidal and subtidal area (shallower than −5 m isobaths) reached 2400 km^2 in 2010. The subaerial delta is densely populated and highly developed, has a mean elevation of about 2 to 4 m above mean sea level, and is significantly affected by land subsidence with an annual rate up to 20 mm between 1970 and 2010 (Dong *et al.*, 2014).

Over the past millennium, the Nanhui Shoal and Nanhui tidal flat prograded south-eastward with a mean subaqueous slope of 1/3000, leading to the formation of the largest marginal intertidal flats near the South Passage (Chen *et al.*, 1988; Dai *et al.*, 2008) (Fig. 1B). The sediment load from the Changjiang River reaches the subaqueous delta and Hangzhou Bay through this shoal–channel system (Yun, 2004). The tidal regime is controlled by irregular semidiurnal tides, tidal deformation and shallow constituents both increase landward (Chen *et al.*, 2001; Zhang *et al.*, 2018). The maximum and mean tidal ranges are 5.1 m and 2.9 m at the offshore entrance of the delta distributary, and the mean tide level is usually 0.3 to 0.5 m higher in summer than that in winter (Chen *et al.*, 1988; Yun, 2004). The tidal current runs south-east–north-west and parallel to bathymetric isobaths on the north side of the Nanhui Shoal, while showing a clockwise rotating flow on the east side (Li *et al.*, 2010). The wave climate on the shoal is influenced by the East Asian monsoon; waves are mainly produced by winds followed by swells, which come from the SSE in summer and from the north-west/north-east in winter (Chen *et al.*, 1988; Dai *et al.*, 2015). The mean and maximum wave heights at Dajishan station (Fig. 1B) are 0.8 m and 7.0 m, respectively (Yun, 2004). In Nanhui Shoal and tidal flats, the depth-averaged suspended sediment

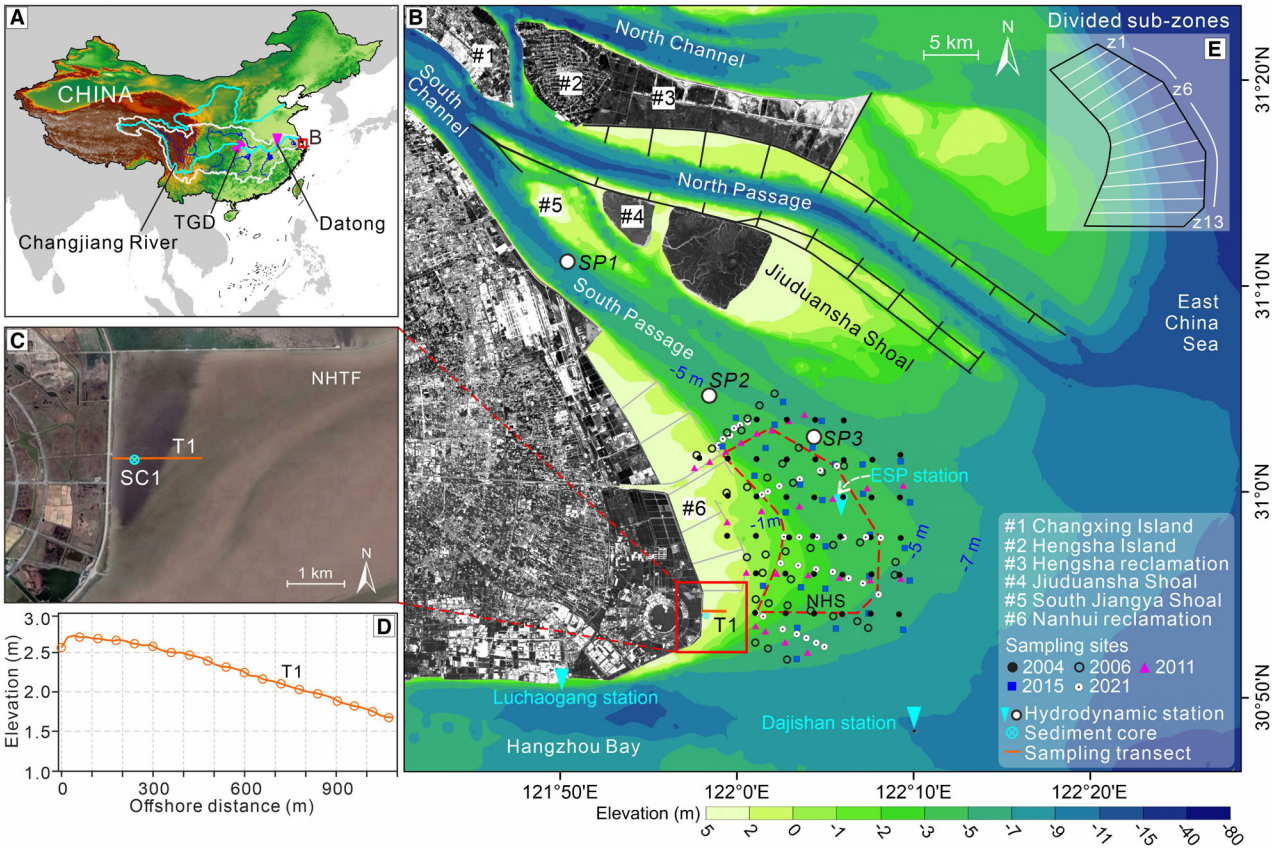

Fig. 1. (A) Location and tributaries of the Changjiang River Basin, showing the Three Gorges Dam (TGD) and Datong hydrological station (limit of tidal wave propagation). (B) Study area and sediment sampling sites, the red dotted polygon represents the Nanhui Shoal (NHS) which encloses the subaqueous sediment sites sampled in five periods; the red rectangle represents the Nanhui tidal flat (NHTF) enclosing a sampling transect and a sediment core, the hydrodynamic gauging stations are also indicated. (C) and (D) Location of the intertidal sampling transect and elevation of the sampling site. (E) The Nanhui Shoal was longitudinally divided into 13 sub-zones (*z*1 to *z*13) from upstream to downstream, to examine longitudinal bathymetric and sedimentary variations.

concentrations (SSCs) during the flood period are higher than those during the ebb period.

Extensive artificial reclamations and hydraulic engineering were carried out along the south flank of the Changjiang Delta in recent decades. The entire supratidal and parts of the intertidal zone have been transformed into artificial land that is isolated by seawalls and groynes, thus inevitably affecting the hydro-sedimentary environment (Li *et al.*, 2010; Wei *et al.*, 2019). The latest siltation-promoting project was implemented in the upper–middle intertidal zone starting in 2014 (Fig. 1B). Herein, the variations in bottom sediments and morphodynamic adaptation of Nanhui tidal flat and Nanhui Shoal related to a declining riverine sediment load and a rising sea level were examined.

DATA ACQUISITION AND METHODS

Data acquisition

Sediment sampling in the Nanhui Shoal and Nanhui tidal flat

To analyse the sedimentary characteristics and shifts of the tidal flats and shoal, a total of three sets of sediment samples were acquired.

1 Large-scale surficial sediments in the Nanhui Shoal were collected along multiple transects in 2004, 2006, 2011, 2015 and 2021, the total number of sampled bottom sediments was 32, 35, 25, 28 and 34, respectively (Fig. 1B). All sediments were sampled with a shipborne bottom sediment grab sampler during the end of

the flood season, the locations and water depths of sampling sites were recorded simultaneously using a Trimble DGPS (Differential Global Positioning System; Trimble Inc., Westminster, CO, USA) device and a single-beam echosounder (ATLAS DESO 17; Atlas Hydrographic GmbH, Bremen, Germany) (Dai *et al.*, 2008; Yan *et al.*, 2009).

2 Intertidal surficial sediments along a fixed repeat transect (named T1) were obtained between April 2018 and December 2021. During all sampling periods, only the topmost 0.5 to 1.0 cm of surficial sediments were collected manually during the lowest tides when the intertidal zone was exposed. The sampling interval of each site was kept at *ca* 60 m and the longest seaward distance reached 1600 m; the intertidal transect presents an upwardly convex topographic profile with a slope of 1/900 (Fig. 1C and D).

3 An intertidal sediment vibracore (named SC1, with a length of 85 cm) was extracted in the Nanhui tidal flat approximately 200 m offshore in July 2018.

Bathymetric data of the Changjiang Delta

To characterize geomorphic patterns and changes, high-resolution bathymetric datasets around the Nanhui Shoal and adjacent subaqueous delta were acquired in 1990, 2004, 2010, 2015, 2019 and 2021, with a scale ranging from 1:10 000 to 1:25 000. During the bathymetric surveys, a DGPS device (Trimble Inc.) and a shipborne dual-frequency echo sounder (ATLAS DESO 17) was used to measure the tidal corrected water depth and site position. The vertical and horizontal errors of measurements are 1.0 and 0.1 m, respectively (Mei *et al.*, 2018a). All bathymetric datasets were provided by the Changjiang Delta Waterway Administration, Chinese Ministry of Transportation. Multi-period digitized sounding points were projected to the Beijing-1954 coordinate, the measured elevations were referenced to the Wusong datum (lowest tide level in Changjiang Delta).

Fluvial material supply from the Changjiang River

To assess variations in the total amount and nature of fluvial material input from the Changjiang River in recent decades, annual water discharge and suspended sediment discharge, and monthly suspended sediment concentration at Datong hydrological station (tidal limit) during the 1950s to 2020 were obtained. The monthly and annual average and maximum grain size of suspended sediments at Datong were also acquired from 2002 to 2017. All data were recorded and provided by the Changjiang River Water Resources Commission, the Ministry of Water Resources China.

Deltaic hydro-sediment dynamics

To discern the variations in hydro-sediment dynamics in the Changjiang Delta, a total of four well-representable datasets were collected herein.

1 The diversion proportions of riverine water discharge and suspended load that flow into the South Passage since 1982 were acquired from the Changjiang Estuary Waterway Administration Bureau and compared to the values for the North Passage (two tributaries downstream from the South Channel) (Fig. 1B).

2 Hourly water levels at the East South Passage tidal gauging station were adopted from 2003 to 2019 to investigate the changes of tidal regime around the Nanhui Shoal. The monthly/annual high, low and mean tidal levels and tidal range were also calculated.

3 Anomaly of extreme wave height at the Dajishan station (Fig. 1B) between 1979 and 2019 was acquired from the Blue Book on Oceanic Climate Change in China (2021).

4 Depth-averaged SSC in August near the East South Passage station between 2002 and 2019 and SSCs at three fixed observation sites along the South Passage between 2006 and 2017 were obtained (Fig. 1B). Specifically, the SP1 site was located upstream of the South Passage, and the SP2 and SP3 sites were near the Nanhui Shoal (Fig. 1B).

Historical shorelines and satellite images

To illustrate the south-eastward advance process of subaerial land in the southern chenier plain of the Changjiang Delta, the historical seawalls were delineated between 713 AD and 1979, including the six seawalls stacked with clods and stones to resist storm surges (Mao *et al.*, 2014). The shorelines and newly constructed seawalls/groynes in the recent four decades were also digitized based on Landsat satellite images. These images describe artificial reclamations and siltation-promoting projects that occupied the supratidal and upper–middle intertidal zones. Finally, satellite imagery was used to track the colonization and rapid expansion of salt marshes within the reclaimed areas from August 2013 to August 2022. All of the data characteristics and acquisition dates are shown in Table 1.

Methods

Sediment grain-size measurements

All surficial sediment samples collected in the Nanhui tidal flats and subtidal Nanhui Shoal were pre-processed before grain-size analyses in the laboratory (Sperazza *et al.*, 2004). For each sample, 10% hydrogen peroxide and 10% hydrochloric acid were added to remove organic matter and calcium carbonates. After adding 5% sodium hexametaphosphate, the samples were placed into an ultrasonic shaker for 20 min to facilitate disaggregation. Sediment grain size was measured in the laboratory using the Malvern Mastersizer 2000 (Malvern Panalytical, Malvern, UK) based on the principle of laser diffraction (Ryżak & Bieganowski, 2011). The Folk and Ward graphical methods (Folk & Ward, 1957) were applied to calculate grain-size parameters of each sediment, including sand/silt/clay fractions, average grain size (X_{average}), sorting coefficient (δ), skewness (Sk) and kurtosis (Ku) (Appendix S1). In addition, the clay (0.5 to 4.0 μm), silt (4.0 to 62.5 μm) and sand (62.5 to 200.0 μm) fractions were also calculated, and all sediments were classified and named according to the Shepard naming rules (Folk & Ward, 1957).

Intertidal sedimentation rate

The sediment core was sliced at 1.0 cm intervals, and all sliced sediment samples were dried and crushed. Biodetritus and vegetation roots were removed with a 40-mesh sieve. Some sediments were selected and sealed in a plastic box, and placed in a cabinet with a dry and undisturbed environment for at least 20 days to reach equilibrium between ^{226}Ra and its daughter nuclides. Then, the specific activity of ^{210}Pb (46.5 keV) and ^{226}Ra (351.9 keV) were measured using a high-purity gamma-ray germanium spectrometer (Canberra Be3830, 777 lead shield; Mirion, Atlanta, GA, USA) (Mei *et al.*, 2018a). Afterwards, the specific activity of excess ^{210}Pb (^{210}Pb$_{ex}$, the difference between the specific activity of ^{210}Pb and ^{226}Ra) was calculated. The average sedimentation rate was determined using a constant initial concentration (CIC) model as in Eq. 1 (Michels *et al.*, 1998; Andersen *et al.*, 2000):

$$\mathrm{Sr} = {}^{\lambda z}\!/_{\ln(A_0/A_z)} \tag{1}$$

where Sr is sedimentation rate (cm/year), z is the depth of sediment (cm), λ is the decay constant of ^{210}Pb (0.031 year^{-1}), A_0 and A_z are the

Table 1. Statistics of data categories, items and corresponding dates used in this study. SSC = suspended sediment concentration.

Category	Item	Date (number)
Sediments	Nanhui Shoal	September 2004 (32), September 2006 (35), September 2011 (25), September 2015 (28), September 2021 (34)
	Nanhui tidal flat	April 2018 (10), July 2018 (17), January 2019 (17), July 2019 (17), July 2020 (27), December 2021 (17)
	Intertidal core	July 2018 (1)
Bathymetries	Subaqueous	1990, 2004, 2010, 2016, 2019, 2021
Fluvial inputs	Water discharge	1950s to 2020
	Discharge and concentration of suspended sediment	1950s to 2020
	Average and maximum grain size of suspended sediment	2002 to 2017
Deltaic hydro-sediment dynamics	Diversion proportions of water and sediment discharge	Since 1982
	Tidal level and range	2003 to 2019
	Extreme wave height	1978 to 2019
	Subtidal SSC	2002 to 2019
	Deltaic SSC	2006 to 2017
Historical information	Shorelines and seawalls	Since 713 AD
Satellite images	Landsat 4–8	Since 1986

specific activity of $^{210}Pb_{ex}$ of surface and z-depth sediment.

Spatial characteristics of subtidal sedimentary patterns

The Natural Neighbour Interpolation (Sibson, 1981) was used to produce spatial distributions of sediment grain-size parameters (average grain size, sorting coefficient and skewness) in the Nanhui Shoal from 2004 to 2021. The spatial patterns of the three parameters were divided into different grades according to the same classification criteria and the area proportion of each grade was calculated. Thus, Shannon's diversity index (SHDI, Eq. 2, Yarnell *et al.*, 2006) was adopted to characterize the heterogeneity of bottom sediment changes during different periods:

$$\mathrm{SHDI} = -\sum_{i=1}^{m} p(x_i) \times ln[p(x_i)] \tag{2}$$

where $p(x_i)$ is the area proportion of grade i in the entire Nanhui Shoal and m is the total number of grades. The SHDI reflects the heterogeneity of spatial characteristics and is sensitive to a non-equilibrium distribution of sediment grain-size parameters. When SHDI = 0, one grade occurs in the entire study area. A high SHDI value indicates that the different grades are more separated, with a greater fragmentation degree and more uncertain spatial information (Uuemaa *et al.*, 2008; Shi *et al.*, 2013).

In addition, the contagion index (CONTAG, Eq. 3) also was applied to quantify the spatial contagion of grain-size parameters in the Nanhui Shoal (Qi *et al.*, 2014):

$$\mathrm{CONTAG} = \left[1 + \frac{\sum_{i=1}^{m}\sum_{k=1}^{m}\left[p(x_i)\left[\frac{g_{ik}}{\sum_{k=1}^{m} g_{ik}}\right]\right] \bullet \left[\ln\left(p(x_i)\right)\left[\frac{g_{ik}}{\sum_{k=1}^{m} g_{ik}}\right]\right]}{2\ln(m)}\right] (100) \tag{3}$$

where $p(x_i)$ is the area proportion of grade i, m is the total number of grades and g_{ik} is the probability that two random adjacent locations belong to grades i and k. Specifically, the $0 < \mathrm{CONTAG} <= 100$ represents the agglomeration degree or extension of different grades. A high value indicates the presence of some dominant grades with greater connectivity in the Nanhui Shoal, otherwise, the spatial pattern of sediment grain-size distribution has small patches (Uuemaa *et al.*, 2007; Qi *et al.*, 2014).

Analysis of bathymetric changes

Three transects were set up around the Nanhui Shoal and adjacent subaqueous areas to analyse bathymetric changes. Specifically, according to hydrodynamics and geomorphological features, the Nanhui Shoal was longitudinally divided into 13 sub-zones ($z1$ to $z13$), to examine variations in sediment distributions and bathymetric depths (from −1 to −6 m isobaths at a 0.5 m interval) during different periods (Fig. 1E). The Natural Neighbour Interpolation was used to produce the digital elevation models (DEMs) in the Nanhui Shoal and subaqueous delta, all DEMs were referenced to the Wusong datum in the Changjiang Delta (the local theoretical lowest tide level) (Wang *et al.*, 2020). Hence, bathymetric changes as well as erosion and deposition patterns were obtained by subtracting two subsequent DEM layers in geographic information software (Mei *et al.*, 2018b) (Eq. 4):

$$\Delta E(x, y, t_1, t_2) = E_2(x, y, t_2) - E_1(x, y, t_1) \tag{4}$$

where $E_1(x, y, t_1)$ and $E(x, y, t_2)$ are bottom elevations at any DEM position (x, y) at times t_1 and t_2. Thus, the areas and volumes of erosion/deposition and corresponding net geomorphic changes during different periods were calculated.

Hydrodynamics model

A two-dimensional Delft3D model was used to simulate the hydrodynamic characteristics in the Changjiang Delta in different years and under changed riverine and marine conditions. First, measured bathymetry and three runoff inputs (incremental in magnitude) were prescribed to model the monthly average hydrodynamics in 2004 and 2020, respectively. Second, the hydrodynamics following sea-level rise (0.1 to 1.0 m) in 2020 were modelled when the runoff input was set at 50 000 m^3. In this study, the well-validated model was run for a total of 10 different scenarios.

The model domain covered the lower reaches of the Changjiang River, its delta, and parts of the East China Sea/Yellow Sea to the −80 m isobath. To avoid errors caused by boundary effects, the east–west and north–south distances of the domain reached 700 km and 560 km, respectively (Wang *et al.*, 2022b). The grid resolution in this study was *ca* 200 to 300 m around the Nanhui

Shoal and South Passage, which meets the needs for accurate hydrodynamic simulations (Zhang *et al.*, 2018). All artificial groynes and dykes of the siltation-promoting projects in the Nanhui tidal flat, shoal and the Deep-water Navigation Channel in the North Passage (Fig. 1B) were regarded as a Current Deflection Wall in Delft3D. The time step was 60 s to meet CFL (Courant–Friedrichs–Lewy) criteria (Deltares, 2014), and the simulation period was from July to August. More detailed descriptions of model setup and calibrations (water level, flow direction and velocity) are provided in Wang *et al.* (2022b).

Herein, both the open boundary conditions for the upland (runoff input at the upstream Datong station) and oceanside (sea-level rise) were changed. Different bathymetries of the Changjiang Delta were measured in 2004 and 2020, respectively, and then adopted in this hydrodynamic model with the same grid. The varying riverine inputs (in 2002 and 2020) and marine boundaries (in 2020) were used in different scenarios. Therefore, different scenarios were run with the model.

1 Three constant runoff inputs (20 000 m^3, 50 000 m^3 and 80 000 m^3) at Datong station in both 2004 and 2020. They correspond respectively to about 1%, 60% and 100% of the cumulative frequency of monthly water discharge (based on hydrological results over the past 60 years). These scenarios were called $Q_{20\ 000}$, $Q_{50\ 000}$ and $Q_{80\ 000}$.

2 A total of four sea levels (0.1 m, 0.3 m, 0.5 m and 1.0 m) with 13 astronomic–harmonic tidal constituents were prescribed when the runoff input was 50 000 m^3 in 2020. The simulated hydrodynamic results characterize the impacts of sea-level rises, i.e. $Q_{50\ 000\_SL0.1}$, $Q_{50\ 000\_SL0.3}$, $Q_{50\ 000\_SL0.5}$ and $Q_{50\ 000\_SL1.0}$ scenarios. In this work, the effects of wind waves, water salinity and temperature were not accounted for.

RESULTS

Sedimentary variations in the Nanhui tidal flats

Vertical sediment variations in the core

The $^{210}Pb_{ex}$ activity in the intertidal sediment core collected in the Nanhui tidal flat declines logarithmically with increasing burial depth between 18 cm and 80 cm (Fig. 2A). The activity fluctuations indicate the potential variability of intertidal sedimentary processes, and a mean

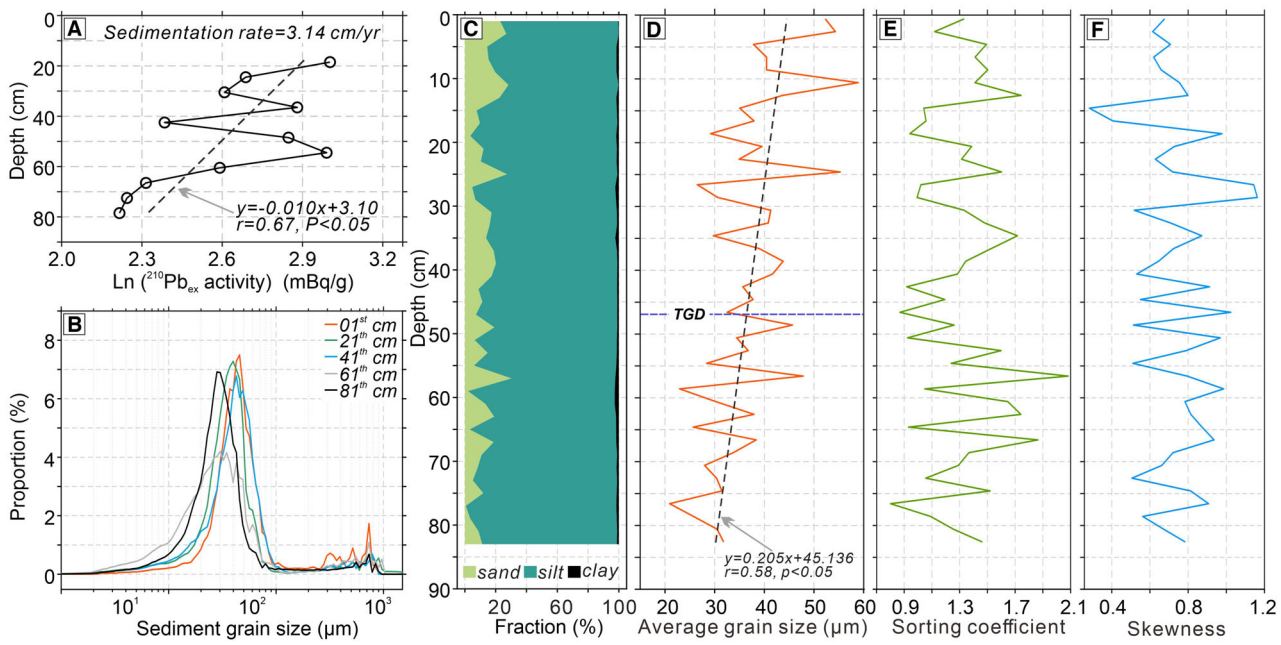

Fig. 2. (A) Vertical variation in radioactive $^{210}Pb_{ex}$ activity in a sediment core collected in the Nanhui tidal flat, and (B) the frequency of different grain sizes at different depths. (C) to (F) Vertical variations in sand–clay–silt fractions, average grain size, sorting coefficient and skewness in the sediment core.

sedimentation rate of 3.1 cm/year was calculated overall (Fig. 2A). From the bottom to the surface, the grain-size frequency curve of the buried sediments gradually shifts from bimodal to multimodal, although the proportion of coarse-grained peaks is low overall (Fig. 2B). The position of fine-grained peaks indicates a progressive coarsening-upward with depth (Fig. 2B). The sand fraction increases with decreasing silt fraction near the surface, while the clay content is very low in the entire core (<3.0%) (Fig. 2C). As a result, sediment grain size coarsens upward, with a general increasing trend after the construction of the TGD in 2003 (Fig. 2D). The overall mean sediment grain size is 32.2 μm during the pre-TGD period (between 1990 and 2003) with a standard deviation of 6.5 μm, both increase to 40.2 μm (coarsened by 24.8%) and 8.6 μm during the post-TGD period (between 2004 and 2018), respectively (Table 2). Sorting and skewness coefficients slightly decreased by 1.5% and 9.2% after the TGD, displaying fewer fluctuations (Fig. 2E and F; Table 2).

Table 2. Mean values and standard deviations (SD) of grain-size parameters in the intertidal sediment core collected in the Nanhui tidal flat. TGD = Three Gorges Dam.

	Average grain size (μm)		Sorting coefficient		Skewness	
Period	Mean	SD	Mean	SD	Mean	SD
Pre-TGD	32.18	6.54	1.31	0.33	0.76	0.18
Post-TGD	40.15	8.64	1.29	0.23	0.69	0.22
All	36.54	8.49	1.30	0.28	0.72	0.20

Characteristics of surficial sediments along the intertidal transect

In April 2018, the average grain size of intertidal surficial sediments in the Nanhui tidal flats increased from 40.4 μm at the most landward site to 46.0 μm at 60 m offshore, then dropped to 28.6 μm between 60 to 180 m, and gradually coarsened again seaward (Fig. 3A). After tropical cyclone Ampil landed in the Changjiang Delta on 22 July 2018, the average grain size increased overall by 29.8%, displaying more transverse fluctuations with a standard deviation of 7.67 μm (Fig. 3A; Table 3). In January 2019, the overall average grain size decreased to 34.3 μm,

Table 3. Monthly mean values and standard deviations (SD) of grain-size parameters of intertidal surficial sediments collected in the Nanhui tidal flat.

	Average grain size (μm)		Sorting coefficient		Skewness	
Date	Mean	SD	Mean	SD	Mean	SD
July 2018	51.88	7.67	1.66	0.17	2.79	0.28
January 2019	34.27	5.55	1.68	0.33	2.50	0.35
July 2019	40.23	4.57	1.74	0.22	2.76	0.31
July 2020	28.49	7.91	1.39	0.24	0.74	0.29
December 2021	41.00	2.59	1.04	0.17	0.45	0.23

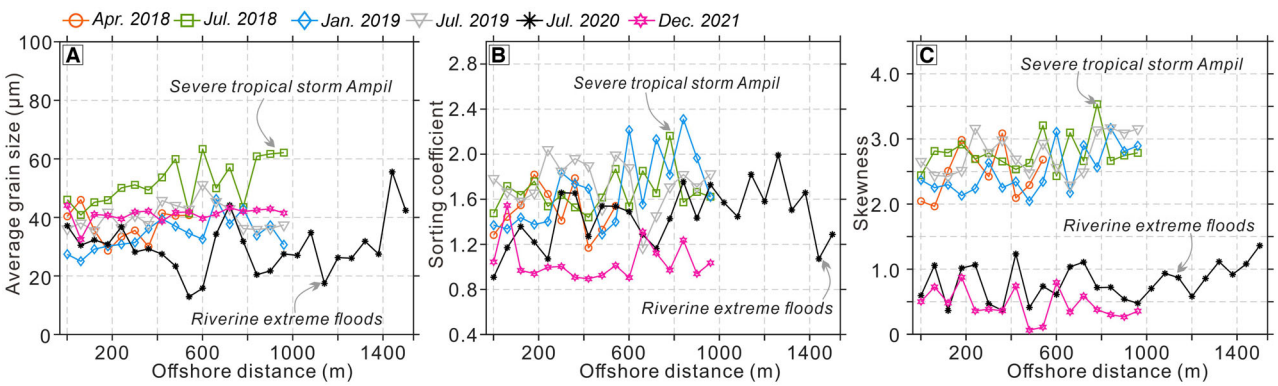

Fig. 3. Transverse distributions and variations in: (A) average grain size; (B) sorting coefficient; and (C) skewness of intertidal surficial sediments collected in the Nanhui tidal flat from April 2018 to December 2021.

while it coarsened up to 40.3 μm in July 2019; meanwhile, the standard deviation was reduced to 4.57 μm (Fig. 3A; Table 3). During the extreme floods in July 2020, the surficial sediments became finer (except for the site 240 m and 720 m offshore) with an average grain size of 28.5 μm (Fig. 3A). Bottom sediments showed larger spatial fluctuations and the corresponding standard deviation increased to 7.91 μm (Table 3). Excluding the period after tropical cyclone Ampil, the overall average grain size reached a maximum in December 2021 with 41.1 μm and limited transverse variations (Fig. 3A; Table 3).

An increase in the sorting coefficient also occurred in July 2018 after tropical cyclone Ampil, with an overall mean of 1.7 and more pronounced seaward fluctuations (Fig. 3B; Table 3). As the intertidal sediments continued to coarsen in January and July 2019, the sorting coefficient increased in the Nanhui tidal flat (Fig. 3B; Table 3). The sorting significantly decreased to 1.4 after the riverine floods of July 2020, and further reduced to 1.0 in December 2021, indicating that sediments deposited in the Nanhui tidal flats gradually become better sorted (although overall still poorly sorted) with a lower standard deviation (Fig. 3B; Table 3). Moreover, skewness also increased after Ampil in July 2018 and decreased during the extreme floods of July 2020 with an overall mean of 0.7 (Fig. 3C; Table 3). In December 2021 skewness further diminished to 0.5, especially in the middle intertidal zone 480 to 540 m offshore (Fig. 3C; Table 3).

Changes in surface sediments in the Nanhui Shoal

Spatial patterns

In 2004 the average grain size of sediments in the Nanhui Shoal was low; 8 to 16 μm in the northern part near the mouth of South Passage and increasing to more than 20 μm in the southern part, with an overall mean of 18.5 μm (Fig. 4A; Table 4). The proportion of the coarsest fraction (i.e. coarse silt to fine sand, 32 to 110 μm) accounted for 3.1% of the total area (Table S1). In 2006, surficial sediments became finer with an overall mean grain size of 12.6 μm (Figs. 4B and 5A; Table 4). In 2011, two inshore coarse deposits developed with an overall average grain size of 17.3 μm, and the proportion of the coarsest fraction increased to 8.4% (Figs 4C and 5B; Tables 4 and S1). In 2015, medium-fine sediments were present in the northern part, with coarse-grained sediments distributed offshore (Figs 4D and 5C). The overall average grain size increased to 26.0 μm with a peak standard deviation of 14.71 μm, and the proportion of the coarsest fraction grew to 16.5% (Tables 4 and S1). In 2021, this spatial pattern of surficial sediment in the Nanhui Shoal was similar to 2015, with a grain size of 27.3 μm (Figs 4E and 5D; Table 4). The proportion of coarse fraction increased in 2021 to 30.8%, which was 9.8 and 1.9 times higher than in 2004 and 2015 (Table S1). In aggregate, the contours of the grain-size map shifted from perpendicular to shoreline and isobaths in 2004 to parallel in 2021 (Figs 4A to 4E and 5E).

In addition, the sorting coefficient of surficial sediments in the Nanhui Shoal also increased from 1.9 in 2004 to 2.0 in 2021, its corresponding standard deviation became higher from 0.1 to 0.4, and the proportion of area with the worst sorting coefficient (2.1 to 4.0) also rose from 0.7% to 34.0% (Figs 4F to I and 5F to I; Tables 4 and S1). As a result, poorly sorted sediments dominated the northern part of Nanhui Shoal in 2021, while the southern surficial sediments showed a higher sorting coefficient (Fig. 4I). Spatially, the gradual changes in the sorting pattern were consistent with the average grain-size pattern, contours of the sorting coefficient map were also parallel to bathymetric isobaths (Figs 4I and 5I). Skewness of surficial sediments in the Nanhui Shoal decreased sharply in 2021 similar to the decrease in skewness in the Nanhui tidal flats between 2004 to 2021 (Figs 4J to M and 5J to M). The overall mean skewness diminished from 1.6 to 0.2 with a lower standard deviation, indicating that the subaqueous sediments shifted from a very positive to a positive bias during the last two decades, especially in the inshore part and in deep areas (Tables 4 and S1).

Longitudinal and lateral sedimentary shifts

In 2004, the sediment average grain size in the Nanhui Shoal reached a maximum value in the fifth and ninth sub-zones (25.67 μm and 21.37 μm, respectively) (Fig. 6A). In 2006, the grain size in the southern part of the shoal dropped sharply from 23.2 μm to 11.2 μm. In 2011 and 2015, sediments in the northern and central parts of the shoal coarsened, with a maximum of 34.5 μm in the sixth sub-zone in 2015 (Fig. 6A). Sediments further coarsened in 2021, especially in the southern subzones of the Nanhui Shoal, showing more fluctuations between zones (Fig. 6A). Shifts in sorting coefficient and skewness further illustrate that, with the

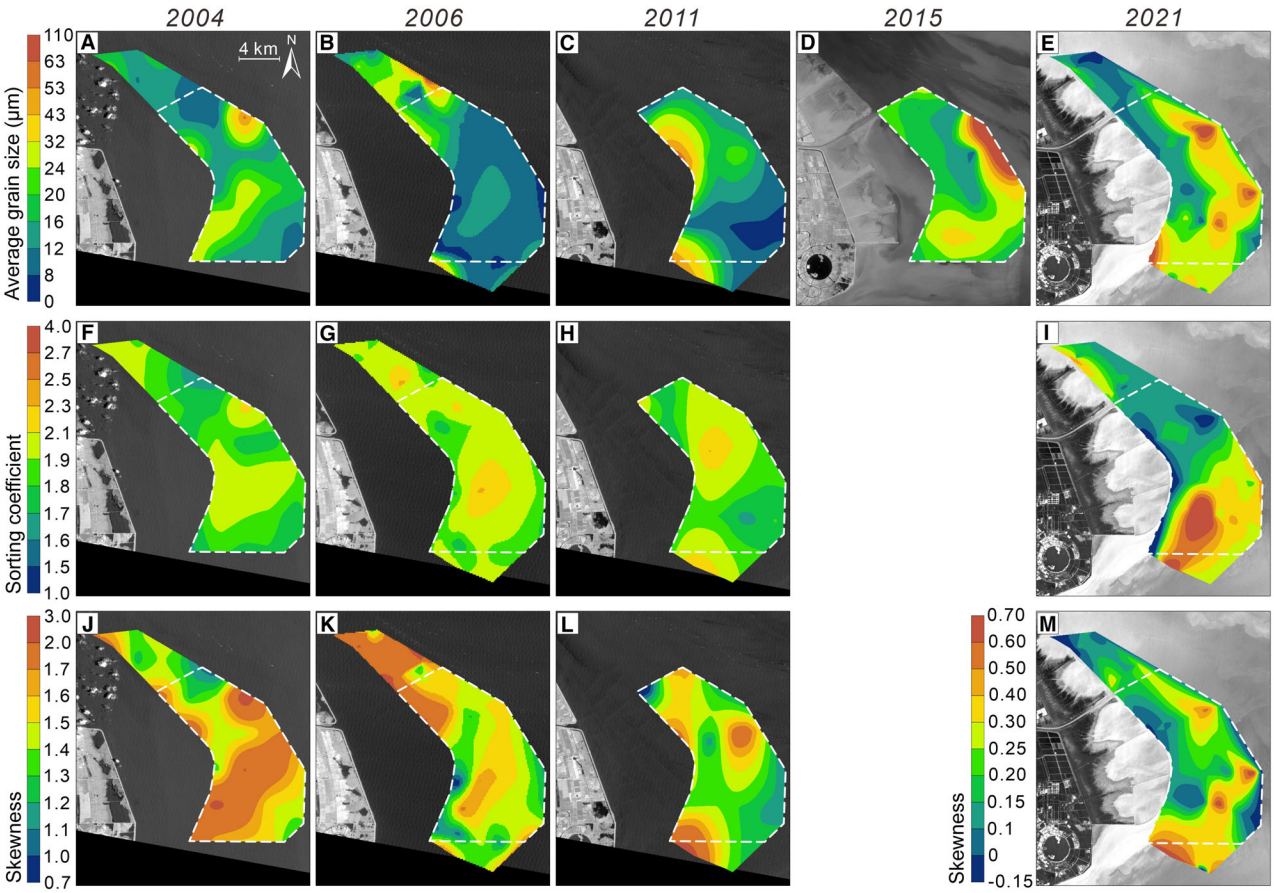

Fig. 4. Spatial patterns of (A) to (E) average grain size, (F) to (I) sorting coefficient and (J) to (M) skewness of surficial sediments sampled in the Nanhui Shoal in 2004, 2006, 2011, 2015 and 2021. Note that a different scale is used for the cumulative difference in (M).

Table 4. Mean values and standard deviations (SD) of three fractions and four grain-size parameters of surficial sediments collected in the Nanhui Shoal.

	Year	2004	2006	2011	2015	2021
Sand fraction (%)	Mean	16.36	3.52	21.98	20.87	25.88
	SD	9.37	2.99	4.63	8.97	14.62
Silt fraction (%)	Mean	67.46	70.41	63.47	58.63	60.44
	SD	6.91	3.83	6.33	7.47	12.50
Clay fraction (%)	Mean	16.18	25.79	14.56	20.49	13.68
	SD	3.20	4.05	10.32	2.66	3.95
Average grain size (μm)	Mean	18.45	12.58	17.27	26.00	27.31
	SD	6.52	4.59	9.35	14.71	12.87
Sorting coefficient	Mean	1.87	1.97	1.90	/	1.96
	SD	0.09	0.10	0.12	/	0.42
Skewness	Mean	1.64	1.48	1.42	/	0.22
	SD	0.19	0.16	0.16	/	0.12

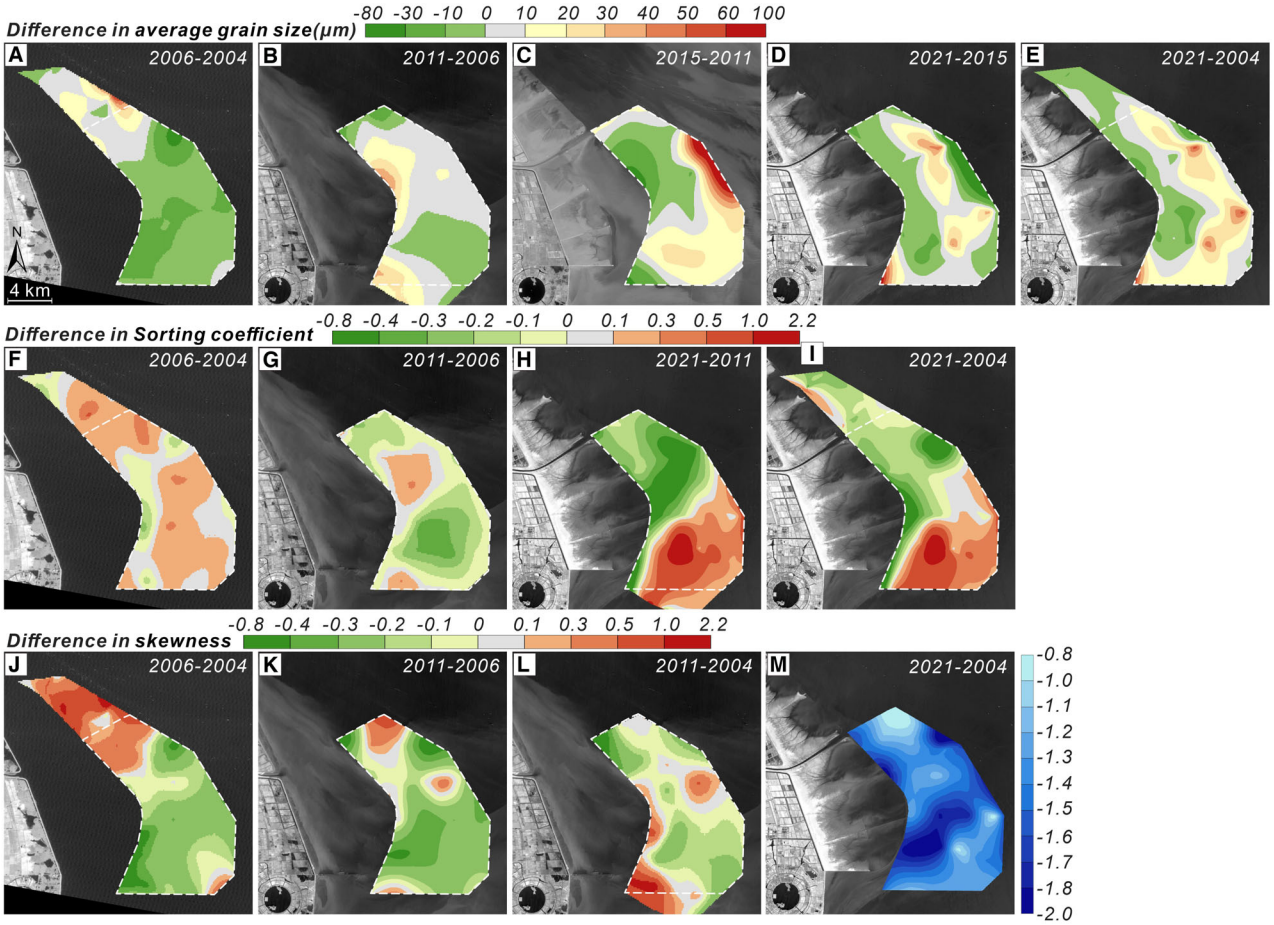

Fig. 5. Spatial patterns of differences in (A) to (E) average grain size, (F) to (I) sorting coefficient and (J) to (M) skewness of surficial sediment collected in the Nanhui Shoal during different periods. Note that a different scale is used for the cumulative difference in (M).

coarsening of surficial sediments, better-sorted material is present in the northern and central areas with an overall decrease in skewness (Fig. 6B and C).

In 2004, sediments in the shallow areas (between −1.5 m and −2.0 m) of the Nanhui Shoal were finer than those of the deep areas (between −5.0 m and −5.5 m), corresponding to a decrease in the average grain size from 28.0 to 11.0 μm (Fig. 6D). In 2006, the sediment grain size was overall finer and the lateral variability was small. However, some shallow areas (< −1.5 m) formed in 2011 and sediments were coarser (47.0 μm), while the grain size in areas deeper than −3.5 m became finer (Fig. 6D). In 2015, the average grain size increased, especially in deep areas, with a peak of 31.8 μm between −4.5 m and − 5.0 m; the peak moved landward in 2021 and gradually developed a bimodal pattern (Fig. 6D). Overall, from 2004 to 2021, surficial sediments in the Nanhui Shoal coarsened especially between −3.0 m and −4.5 m. The sorting coefficient was higher in 2021 (particularly between −1.0 m and −3.5 m) (Fig. 6E), skewness decreased globally and generated a secondary maximum between −2.0 m and −5.5 m (Fig. 6F).

Shannon's diversity index and contagion index of sediment grain size

The SHDI of average grain size of surficial sediments in the Nanhui Shoal dropped from 1.7 in 2004 to 1.3 in 2006 while the CONTAG increased from 54.1 to 62.9, indicating that patches with different values of grain size were less fragmented and were more connected to large-scale patches (Fig. 7A). However, in 2011 SHDI increased to 1.9 and CONTAG decreased to 50.5, showing more partitioned areas with

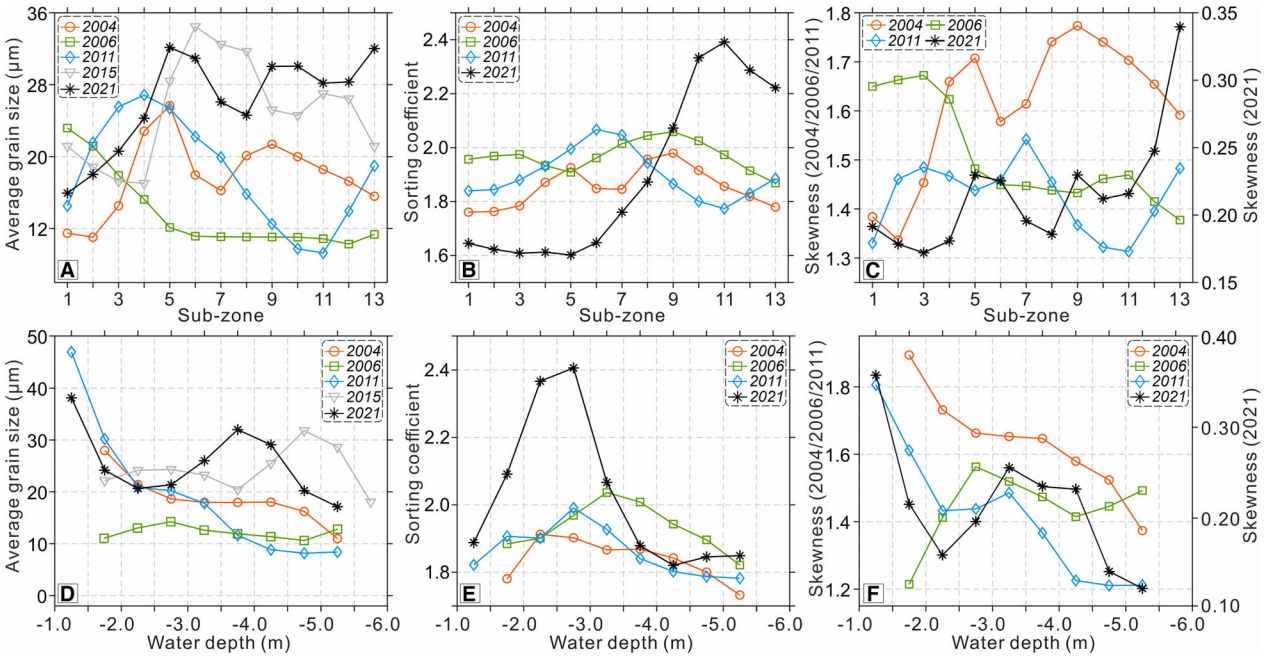

Fig. 6. Mean values of average grain size, sorting coefficient and skewness of surficial sediments in different (A) to (C) divided sub-zones and (D) to (F) bathymetric depths.

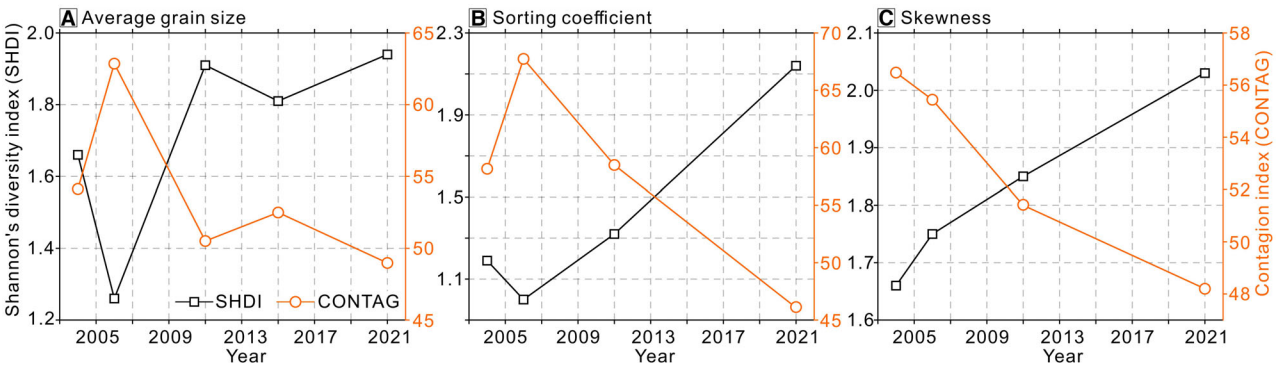

Fig. 7. The Shannon's diversity index **(**SHDI) and contagion index (CONTAG) values of the distributions of sediment average grain size, sorting coefficient and skewness in the Nanhui Shoal.

similar values. The spatial patterns were maintained in 2015 and were further enhanced in 2021 (Fig. 7A). Thus, compared with 2004, more scattered patches of high and low grain-size values were formed in the Nanhui Shoal; SHDI increased by 16.9% and CONTAG decreased by 9.5% between 2004 and 2021 (Fig. 7A). Consistent with the variations in average grain size, the SHDI of both sorting coefficient and skewness of sediments increased (by 79.8% and 22.3%), while CONTAG decreased (by 20.7% and 14.7%), illustrating that the spatial distribution of sediment characteristics in the Nanhui Shoal became more fragmented and less organized (Fig. 7B and C).

Morphodynamic changes

Spatial patterns of bathymetry

Isobaths around the Nanhui Shoal protruded south-eastward with relatively equal spacing in 1990 (Fig. 8A). The shallowest areas were

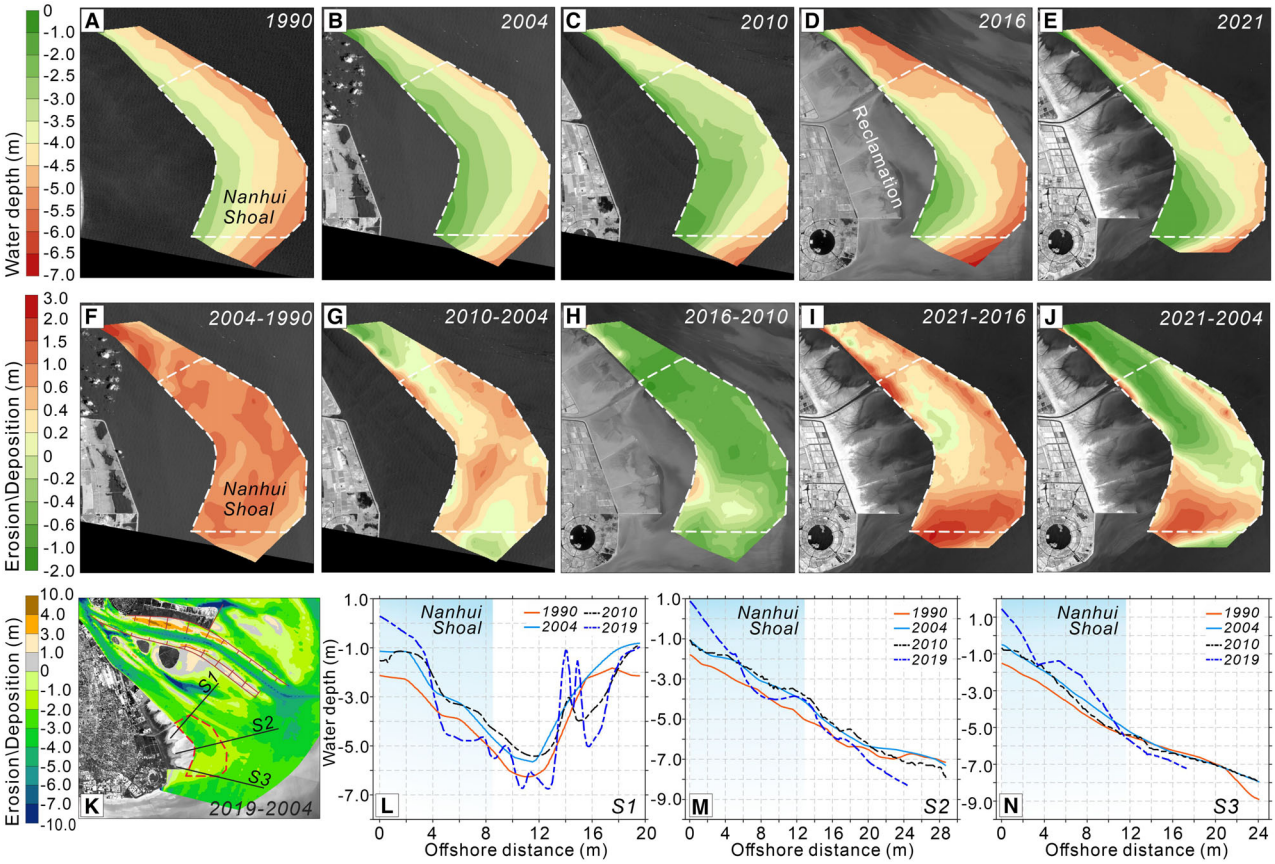

Fig. 8. (A) to (E) Water depth in the Nanhui Shoal in 1990, 2004, 2010, 2016 and 2021, and (F) to (J) erosion and deposition during different periods. (K) Bathymetric change in the southern Changjiang Delta and (L) to (N) water depth variations along three transects.

Table 5. Maximums, minimums, means and standard deviations (SD) of bathymetries in the Nanhui Shoal during different years.

Year	1990	2004	2010	2016	2019	2021
Maximum (m)	−1.73	−0.89	−0.71	−1.60	−0.39	−0.42
Minimum (m)	−5.69	−5.37	−5.62	−6.76	−6.50	−6.09
Mean (m)	−4.17	−3.44	−3.30	−4.25	−3.82	−3.69
SD (m)	0.69	0.76	0.84	0.99	1.03	1.08

located along the southern boundary, and the maximum, minimum and mean of the bathymetric DEM were −1.7 m, −5.7 m and −4.2 m, respectively (Fig. 8A; Table 5). Between 1990 and 2004, the Nanhui Shoal experienced overall deposition especially in the northern part, with the mean depth increased to −3.4 m (Table 5). As a result, all isobaths advanced seaward and maintained a stable pattern with reduced longitudinal spacing (Fig. 8B and F). After the TGD construction, isobaths continued to move seaward in 2010, but with more spatial fluctuations due to scattered geomorphic erosion and deposition (Fig. 8C and G). In particular, the northernmost and southernmost parts of the Nanhui Shoal suffered severe erosion. In 2016, the

isobaths became more complex due to overall erosion; especially in deep areas, the mean depth increased to 4.3 m (Fig. 8D and H; Table 5). As of 2021, the northern area is still eroded, while deposition has occurred in the southern part promoting shoal progradation that resulted in a mean depth of −3.7 m (Fig. 8E and I; Table 5).

Net deposition in the Nanhui Shoal between 1990 to 2004 was 13.1×10^7 m^3 with a mean accretion rate of 5.2 cm/year (Table 6). During the post-TGD period (2004 to 2010), weaker net deposition occurred with a total deposited volume of 2.6×10^7 m^3 and an annual deposition rate of 2.4 cm/year (Table 7). Specifically, between 2004 and 2021, severe erosion extended longitudinally seaward from the northern part of the Nanhui Shoal, while deposition occurred in the southern part around the shoal corner and extended towards the Nanhui tidal flats (Fig. 8J). Therefore, a distinct demarcation was present in the middle areas, and the standard deviation of bathymetry has continued to increase from 0.7 m in 1990 to 1.1 m in 2021 (Table 5). Except for the severe extensive erosion between 2010 to 2016, the spatial pattern of bathymetric changes in the Nanhui Shoal was different before and after the TGD (Fig. 8F to J).

Table 7. Modelled monthly mean bed shear stresses and corresponding directions in the Nanhui Shoal and the entire study area in different scenarios.

Scenario	Mean bed shear stress (N/m^2)		Mean direction of bed shear stress (°)	
	Nanhui Shoal	Entire area	Nanhui Shoal	Entire area
2004_$Q_{20\ 000}$	0.48	0.52	193.56	199.43
2004_$Q_{50\ 000}$	0.49	0.55	191.84	196.39
2004_$Q_{80\ 000}$	0.51	0.58	190.85	193.72
2020_$Q_{20\ 000}$	0.38	0.47	193.69	198.88
2020_$Q_{50\ 000}$	0.39	0.50	191.85	195.67
2020_$Q_{80\ 000}$	0.42	0.55	190.54	192.78
2020_$Q_{50\ 000\ +\ 0.1m}$	0.40	0.50	191.48	195.55
2020_$Q_{50\ 000\ +\ 0.3m}$	0.40	0.50	190.83	195.35
2020_$Q_{50\ 000\ +\ 0.5m}$	0.40	0.50	190.40	195.29
2020_$Q_{50\ 000\ +\ 1.0m}$	0.41	0.50	190.01	195.59

Morphodynamic stability around the Nanhui Shoal

The southern Changjiang delta exhibited geomorphic change after the TGD construction (Fig. 8K). In the Nanhui Shoal, upstream strong erosion (2.0 to 4.0 m) extended along the ebb-tidal channel (Fig. 8K); however, the intensity of erosion was enhanced (about 2.0 to 4.0 m) in the broad subaqueous delta (Fig. 8K). Along the upstream transect S1, the subaqueous geomorphic complexity increased with more fluctuations in 2021, and the secondary tidal channel further deepened (Fig. 8L). The topographic slope of the shoal at the border with the engineered areas increased sharply (Fig. 8L). Along the middle transect S2, strong erosion (over 2 m) also extended towards the Nanhui Shoal in 2016, the erosion in the deeper area also increased (Fig. 8M). Along the downstream

Table 6. Areas and volumes of erosion (negative) and deposition (positive), and the net bathymetric changes in the Nanhui Shoal during different periods.

Period	Erosion		Deposition		Net volume (10^7 m^3)	Annual thickness (cm/year)
	Area (km^2)	Volume (10^7 m^3)	Area (km^2)	Volume (10^7 m^3)		
1990 to 2004	0.00	0.00	178.93	13.13	13.13	5.24
2004 to 2010	51.29	−1.47	127.43	4.03	2.57	2.39
2010 to 2016	175.50	−16.95	3.26	0.05	−16.90	−15.76
2016 to 2019	24.50	−0.44	154.39	8.13	7.69	14.33
2019 to 2021	51.01	−0.55	124.62	2.21	1.65	4.71
2004 to 2021	106.06	−8.20	69.20	3.56	−4.64	−1.56

transect S3, some deposition was observed within the engineering structures and at intermediate depths in 2021 (Fig. 8N).

Tidal hydrodynamics in different scenarios

Modelled bed shear stress in 2004 when the runoff input was 20 000 m^3/s was higher in the upstream part of the South Passage, and weak along the Nanhui Shoal (from over 0.6 N/m^2 to 0.3 N/m^2) (Fig. 9A). With an increase in runoff to 50 000 m^3/s, the overall bed shear stress increased by 4.6%, and by 11.2% with 80 000 m^3/s (Fig. 9B and C; Table 7). In 2020, the spatial distributions of modelled bed shear stress displayed a strong contrast between the Nanhui Shoal and South Passage (Fig. 9D to F); more patches with low values (<0.3 N/m^2) were generated in the offshore area. Lateral variations in bed shear stress aligned to isobaths in the Nanhui

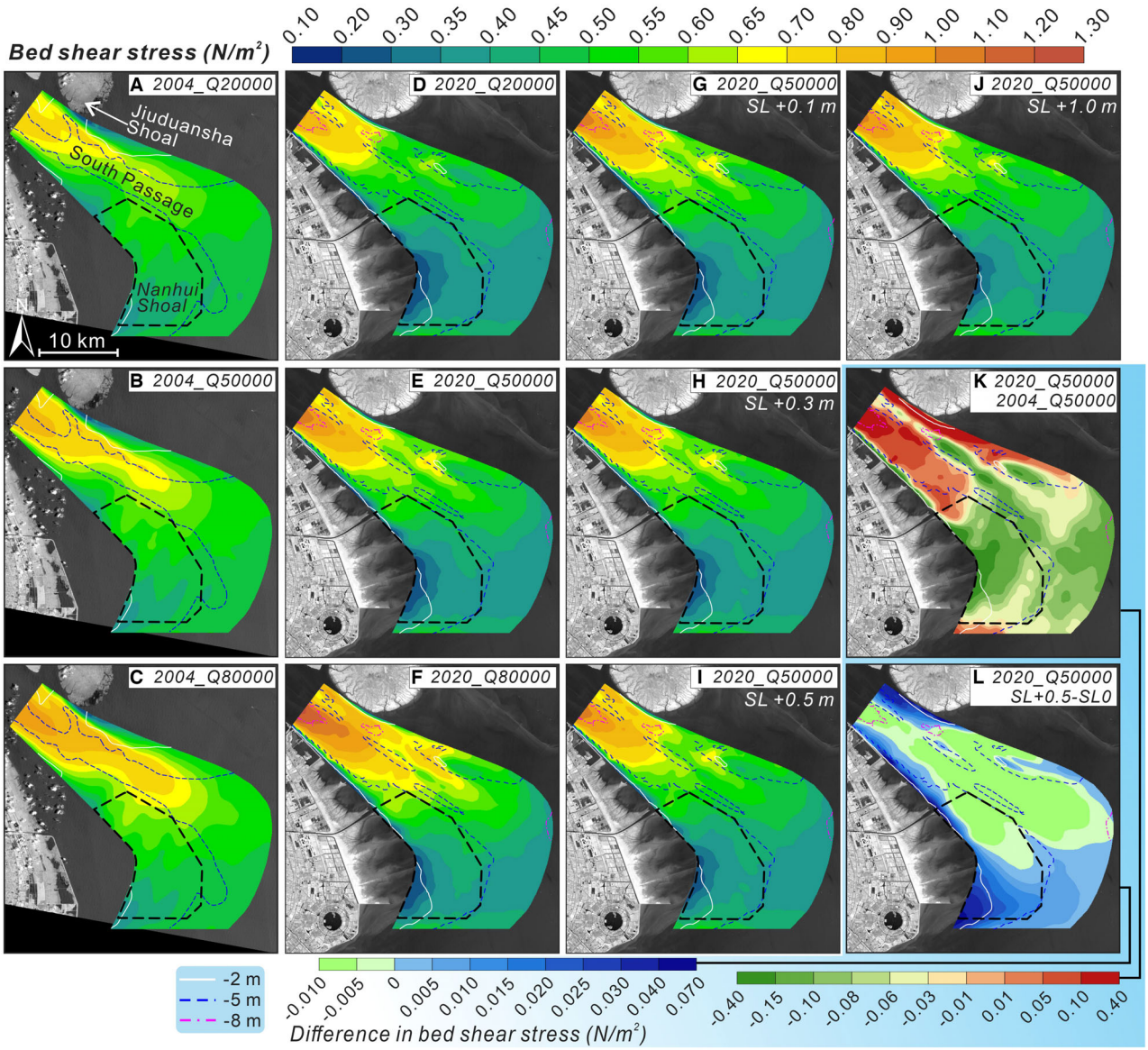

Fig. 9. Modelled mean bed shear stresses around the Nanhui Shoal, South Passage and offshore area under different runoff inputs ($Q_{20\ 000}$, $Q_{50\ 000}$ and $Q_{80\ 000}$) at Datong in 2004 (A) to (C) and in 2020 (D) to (F); (G) to (J) with constant runoff inputs ($Q_{50\ 000}$) and bathymetry in 2020 under four sea levels (0.1 m, 0.3 m, 0.5 m and 1.0 m). (K) Difference between the $Q_{50\ 000}$ scenarios in 2020 and 2004, and (L) difference between $Q_{50\ 000}$ and $Q_{50\ 000\ +\ SL0.5m}$ scenario in 2020.

Shoal (Fig. 9D to F). A comparison of the 50 000 m^3/s scenarios in 2004 and 2020 indicates an increase in bed shear stress in the upstream channel and along the southern side of the Jiuduansha Shoal (Fig. 9K). In addition, when the sea level rose by 0.1 m, 0.3 m, 0.5 m and 1.0 m, bed shear stress in the Nanhui Shoal also increased by 0.25%, 0.7%, 1.5% and 3.5% respectively (Fig. 9G to J; Table 7). Sea-level rise increased bed shear stress in the southern Nanhui Shoal and in the offshore area but decreased along the main channel in 2020 (Fig. 9L).

In the 20 000 m^3/s scenario with the 2004 bathymetry, the direction of bed shear stress was higher than 205.0° in the upstream part of the South Passage, and gradually decreased downstream (Fig. 10A). With the higher runoff input of 50 000 m^3/s and 80 000 m^3/s, the overall shear stress direction decreased (mean was 196.4° and 193.7°, respectively), indicating an enhancement of the ebb tidal current (Fig. 10B to C; Table 7). Directions of bed shear stress in all scenarios were reduced in 2020 compared to 2004, and the difference between upstream and

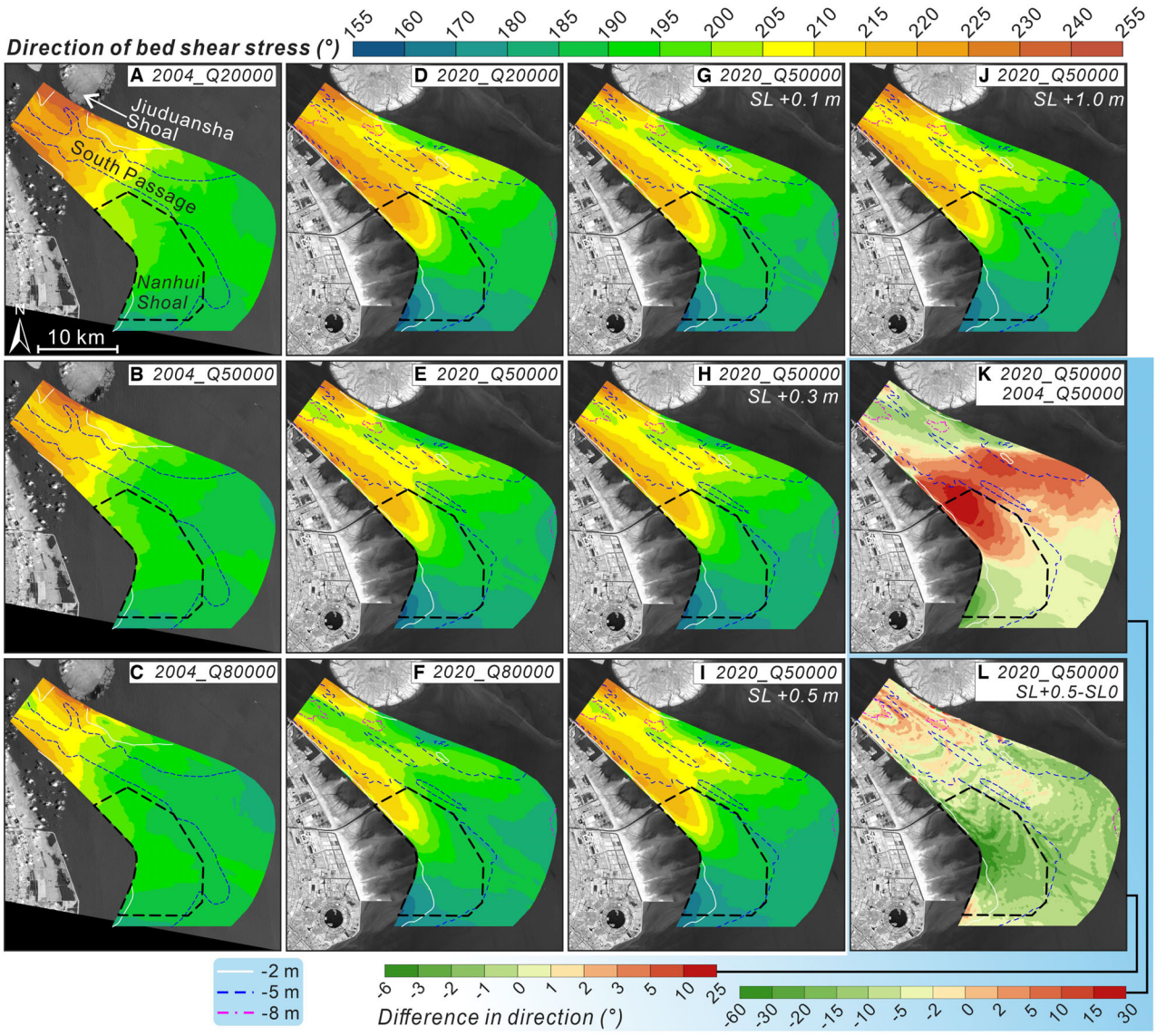

Fig. 10. Modelled mean direction of bed shear stresses under different runoff inputs ($Q_{20\ 000}$, $Q_{50\ 000}$ and $Q_{80\ 000}$) at Datong station in 2004 (A) to (C) and 2020 (D) to (F); (G) to (J) with constant runoff inputs ($Q_{50\ 000}$) and bathymetry in 2020 under four sea levels (0.1 m, 0.3 m, 0.5 m and 1.0 m). (K) Difference between the $Q_{50\ 000}$ scenarios in 2020 and 2004, and (L) difference between $Q_{50\ 000}$ and $Q_{50\ 000\ +\ SL0.5m}$ scenarios in 2020.

downstream was more evident (Fig. 10D to F; Table 7). With sea-level rise, the shear stress directions remained stable (Fig. 10G to J). Sea-level rise led to a decrease in shear stress direction of the offshore area, while it increased in the upstream South Passage.

DISCUSSION

Changes in fluvial sediment supply

In general, fluvial fine-grained sediments are delivered into the delta by runoff and are mostly deposited in marginal tidal wetlands and in subaqueous deltas (Wolinsky *et al.*, 2010; Unverricht *et al.*, 2013). Upstream runoff and sediment inputs dominate the sedimentary processes and the sustainability of mega-deltas, together with the impacts of climate change and human activities (Nilsson *et al.*, 2005; Fagherazzi *et al.*, 2015). Over the past five decades, more than 1.0×10^{10} t of terrigenous sediment transported by 4000 major rivers worldwide has been trapped in dams and reservoirs, affecting the material supply necessary for delta accretion and progradation (Syvitski *et al.*, 2005; Dethier *et al.*, 2022). This reduction has been shown to have caused severe erosion in subaqueous areas and shoreline recession in a couple systems, but it is likely a consistent result (Maloney *et al.*, 2018; Besset *et al.*, 2019). For instance, due to a century-long regulation of riverine inputs, the overall sediment budgets in the Colorado River Delta and adjacent Upper Gulf of California (USA) have been disturbed, and seaward surficial sediments were gradually resuspended and transported upstream (Carriquiry & Sánchez, 1999). The central shoreline of the Indus Delta receded at a mean rate of 50 m/year after a 50% reduction in riverine sediment input since the 1950s (Giosan *et al.*, 2006).

The mean progradation rate of the Changjiang Delta front accelerated around 2000 BP, most likely caused by increased upstream sediment supply related to land-use changes (Hori *et al.*, 2001). After the construction of the Gezhou Dam in 1988 and the Three Gorges Dam in 2003 in the Changjiang River Basin, the annual suspended sediment discharge at Datong station dramatically decreased by 29.4% and 71.9%, compared to the period from the 1960s to the 1980s, although water discharge remains overall stable with some fluctuations (Fig. 11A). The SSC has continued to decline, especially during the flood season, resulting in lower intra-year differences (Fig. 11B) (Dai *et al.*, 2016a). Some studies indicate that the estuarine channels and subaqueous delta front are now characterized by erosion and attributed that to an increase in resuspension of fine-grained sediments due to the sediment-starved tidal currents (Dai *et al.*, 2014; Luan *et al.*, 2016; Zhu *et al.*, 2016; Guo *et al.*, 2021; Luo *et al.*, 2023). However, evidence on how sedimentary characteristics respond to geomorphic variations is still insufficient, especially at large spatiotemporal scales. Herein, results of sediment grain-size analyses indicate that subaqueous surficial sediments in the Nanhui Shoal have been coarsening over the past two decades, and sediment skewness severely reduced (Figs 4A to E and 5A to E; Table 4). In addition, intertidal sediments in the Nanhui tidal flat continued to coarsen (Fig. 6C; Table 4).

The grain-size distribution of terrestrial sediments is also a key factor influencing the sedimentary processes and geomorphic changes in the delta (Orton & Reading, 1993). Due to the trapping of fine-grained sediments in the reservoirs and severe erosion in the middle-lower reaches of the Changjiang River (Dai & Liu, 2013; Mei *et al.*, 2021), the grain size of suspended sediment at Datong station has gradually increased (Fig. S1). As the coarse-grained fraction of discharged riverine sediments increases, the subaqueous shoal topography of the delta became smoother (Edmonds & Slingerland, 2010). Hence, the annual average grain size of suspended sediment coarsened from 0.03 mm in 2003 to 0.05 mm in 2017 (an increase of 82.8%), and the maximum grain size also increased from 0.6 mm in 2004 to 0.8 mm in 2017 (an increase of 46.6%) (Fig. 11C and D). How a coarsened suspended sediment affects the surficial sediments in mega-deltas in the context of decreasing total riverine sediment supply requires more study and understanding (Yang *et al.*, 2014; Dai *et al.*, 2018).

Influence of deltaic hydrodynamic changes on bottom sediments

Hydrodynamics determine the convergence and divergence of suspended and bed sediment fluxes in mega-deltas, thereby influencing the sedimentary characteristics and morphodynamics of shoals and tidal wetlands (Hori *et al.*, 2002; Angamuthu *et al.*, 2018; Leuven *et al.*, 2021). Yamashita *et al.* (2009) emphasized that hydrodynamic spatial and temporal shifts trigger changes in sediment transport in deltaic flats and subaqueous areas. In the Changjiang

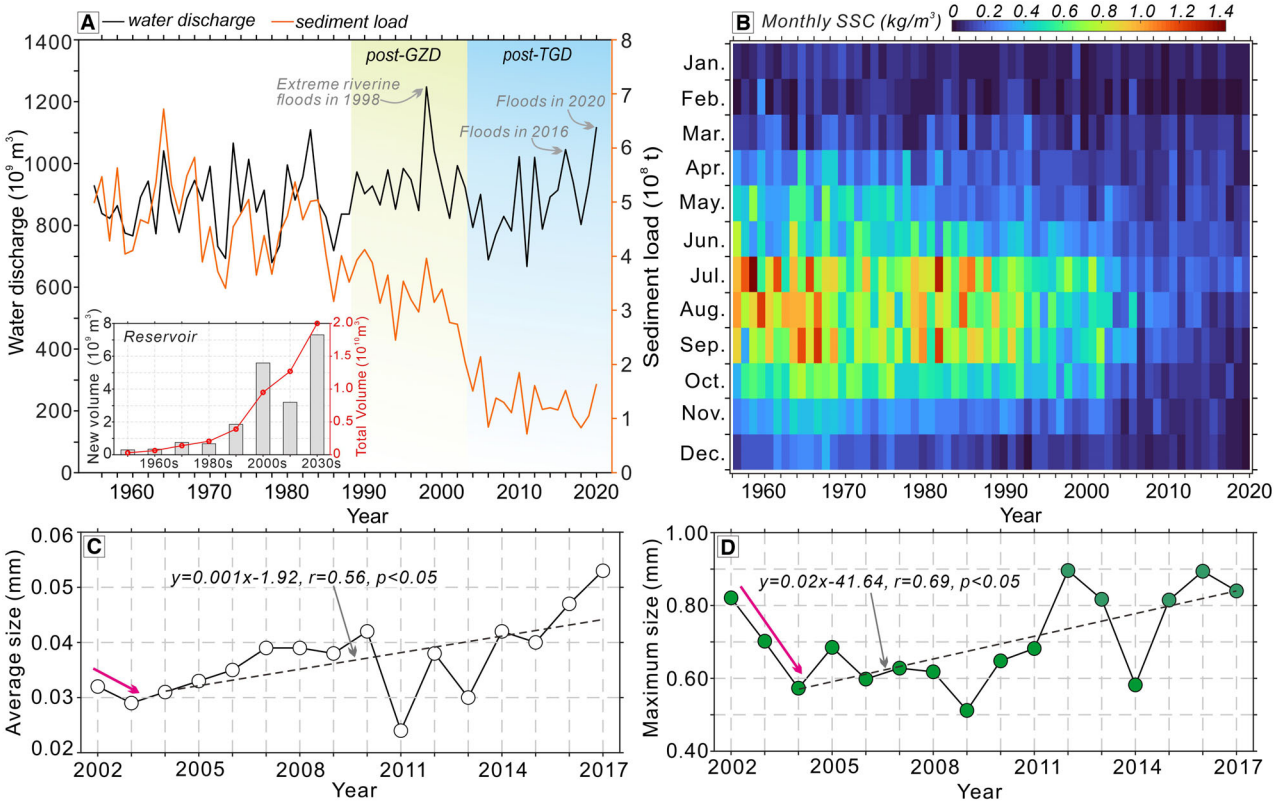

Fig. 11. (A) Total volume of water accumulated in the reservoirs of the Changjiang River Basin and variations in riverine water discharge and suspended sediment discharge at Datong station since the 1950s (GZD–Gezhou Dam; TGD–Three Gorges Dam). (B) Monthly variations in suspended sediment concentration (SSC). (C) and (D) Annual variations in the average and maximum grain size of riverine suspended sediment at Datong station between 2002 and 2017.

Delta, more than one-third of the Changjiang-borne sediments were discharged southeastward through the South Passage and Nanhui Shoal before the TGD, and now this fraction is gradually increasing due to large-scale scour (Chen *et al.*, 2001; Yun, 2004; Dai *et al.*, 2015). In the northern part of the Nanhui Shoal, the hydrodynamics and sediment dynamics are primarily controlled by energetic runoff, that generates the coarse bed sediments in the South Passage (Li, 1991; Li *et al.*, 2010).

In 1998, extreme flooding occurred in the Changjiang River Basin, and the Deep-water Navigation Channel and V-shaped diversion project were constructed in the adjacent North Passage to increase navigation capacity (Fig. 1B). After that, the water discharge and suspended sediment discharge flowing into the South Passage increased, from 37.0% and 42.9% in 1998, respectively, to 58.1% and 64.5% in 2012. Both have remained relatively stable in recent years (Fig. 12). In addition, the bed shear stress was also significantly enhanced upstream in the South Passage between 2004 and 2020 (Fig. 9), which likely promoted the resuspension of fine-grained bed sediments. As a result, the upper main channel of the South Passage and mouth bar have eroded over the past two decades, and most of the eroded sediments are most likely transported downstream (Li, 2018; Zhou *et al.*, 2020).

Tidal forcing controls the net sediment transport in tidal deltas (Scully & Friedrichs, 2007). Recent studies in the Mississippi Delta indicate that sea-level rise and land erosion will strengthen tidal energy, forming wider channels and coarse sediment fractions in the seaward area (Fitzgerald *et al.*, 2004). In the Fly River Delta, rising tidal levels will accelerate tidal wave propagation in the channel network, enhancing tidal asymmetry and sediment resuspension (Scully & Friedrichs, 2007; Canestrelli *et al.*, 2010). Bolla

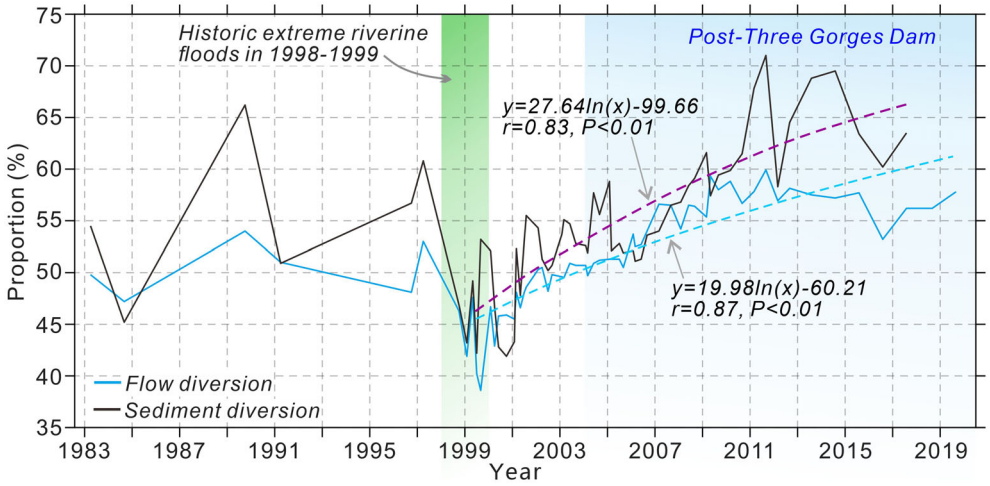

Fig. 12. Changes in diversion proportion of upstream water discharge and sediment discharge that has flowed into the South Passage since the 1980s; historic extreme riverine floods occurred in 1998 and 1999.

Pittaluga *et al.* (2015) used an idealized one-dimensional morphodynamic model (sketch from the Elbe Estuary) and revealed that an increase in tidal range would lead to steeper subaqueous topography and net erosion in tidally controlled deltas.

In the southern Changjiang Delta, the tidal asymmetry first increases and then decreases landward, affecting sediment delivery (Hoitink *et al.*, 2017; Zhang *et al.*, 2018; Mei *et al.*, 2021). The maximum and minimum monthly mean tide level at the East South Passage station in the Nanhui Shoal increased by 20 cm since 2004, and the tidal range also increased significantly (Fig. 13A). Therefore, the annual mean tide level rose by 0.6 cm/year between 2005 and 2019 (Fig. 13B and C). Stronger tidal dynamics will resuspend sediment from deltaic shoals and tidal flats, thereby reducing aggradation rates (Plink-Björklund, 2012). Previous field observations and studies have indicated there was a circulation of that net sediment transport from the Nanhui Shoal to the Nanhui tidal flat (Chen *et al.*, 2001; Yun, 2004; Dai *et al.*, 2008); while the mid-part of the Nanhui Shoal suffers from strong tidal forcing and its surficial sediments are coarser during the past two decades (Fig. S2). In addition, the spatial patterns of sediment grain-size parameters have higher SHDI and CONTAG indexes (Fig. 6), which are most likely attributable to the river sediment reduction and sea-level rise.

Sediment cores analysis In the Nile Delta indicates that the present sedimentation rate is significantly less than the historical long-term rate of 7 mm/year (Frihy, 2003). Rising sea level will induce more sediment erosion in the subaqueous deltas, in particular, the stronger tidal asymmetry along the deltaic channels will lead to net erosion and export of bottom sediments (Lentsch *et al.*, 2018; Leuven *et al.*, 2021). On a long-term scale, sea-level rise and greater tidal range will enhance tidal forcing in most deltas, affecting sedimentary processes of tidal bars and shoals built with fluvial sediments (Plink-Björklund, 2008). Waves also control sediment erosion and geomorphic features in Nanhui Shoal and tidal flat (Mao, 1987; Yang *et al.*, 2002). Wind waves account for about 80% of wave power, and the mean wave height at the Dajishan station was 0.8 m in the Changjiang Delta (Chen *et al.*, 1988; Li *et al.*, 2010). From 1978 to 2004, the anomaly (relative to the mean value between 1993 and 2011) of extreme wave height (the 99th percentile of the 1/10 large wave height) at Dajishan decreased from 1.4 m to −0.3 m, while it increased again after 2004 with a slope of 3.6 cm/year (Fig. 13D). Extreme waves will further trigger scouring, and surficial sediments will coarsen after fine-grained sediments are washed away (Ulses *et al.*, 2008; Harley *et al.*, 2017). This is consistent with maps of sediment convergence and bathymetric changes measured between 2004 and 2020 (Figs. 5E and 8J). More suspended sediments will be delivered into deltaic tributaries during the ebb tidal period, and influence the accumulation and seaward dispersal patterns (Ridderinkhof

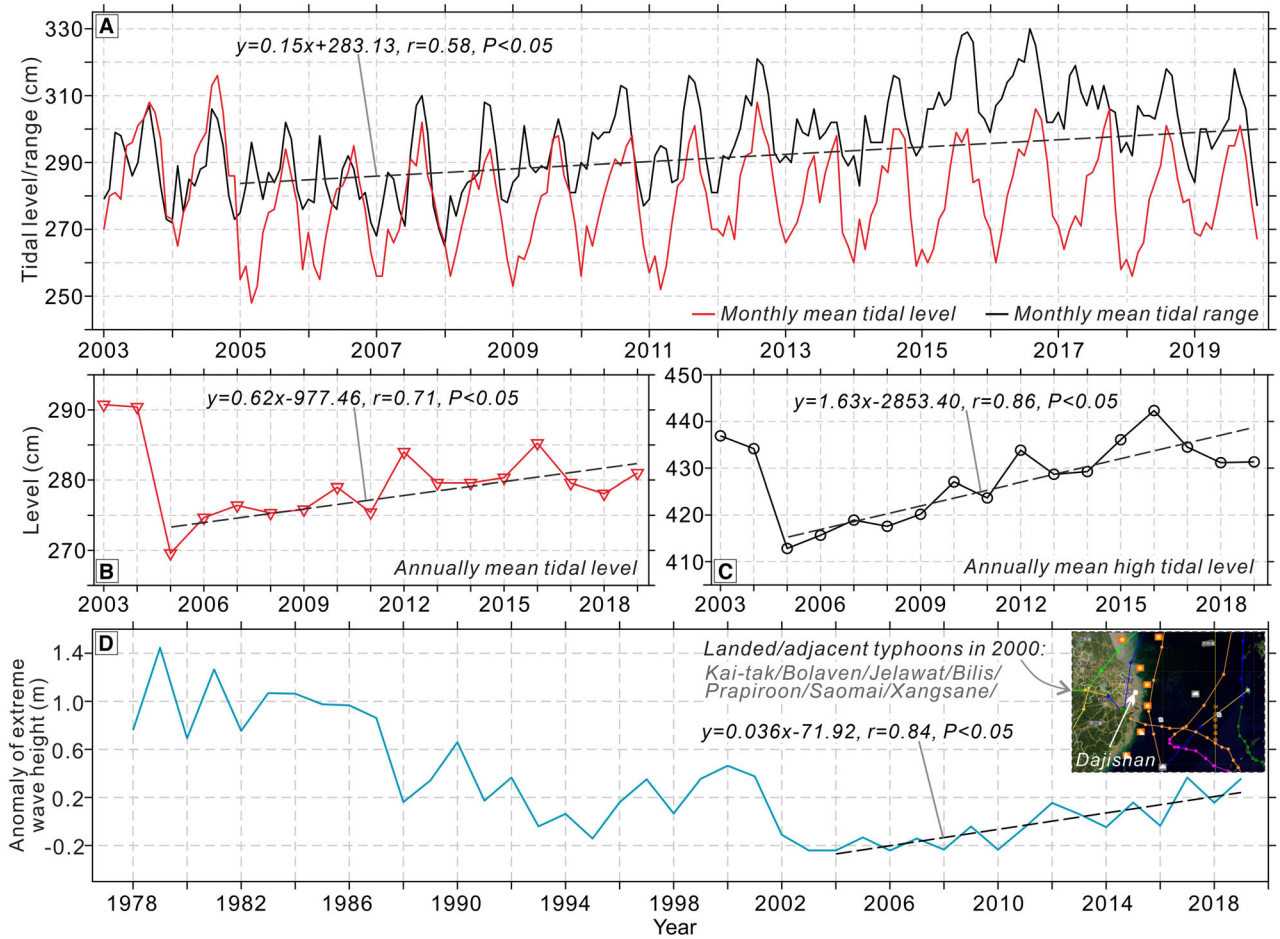

Fig. 13. Variations in (A) monthly mean tidal level/range, (B) annual mean tidal level and (C) annual mean high tidal level at the East South Passage (ESP) hydrodynamic station between 2003 to 2019. (D) Anomaly of the extreme wave height at the Dajishan station since 1978 (from Blue Book on Marine Climate Change in China, 2021).

et al., 2000; Green & Coco, 2014; Walsh *et al.*, 2014).

Transfer of sediments from sources to sinks

The source and abundance of sediments are determinants of sedimentary shifts in the Changjiang Delta based on sedimentary borehole analysis (Hori *et al.*, 2002). For example, the Kapuas River (Indonesia) forms a deltaic channel complex, and Kästner *et al.* (2017) hypothesized that the downstream gradual coarsening of bed sediment inside distributaries was related to upstream insufficient sediment supply. Following a reduction in riverine suspended sediment discharge from the Changjiang River, the SSC of tidal currents around the East South Passage station have continued to decline from 0.9 kg/m^3 in 2002 to 0.4 kg/m^3 in 2019 (Fig. 14A). The SSC at the SP1 site in the South Passage also decreased sharply from 2.2 kg/m^3 in 2006 to a mean of 1.2 kg/m^3 during the 2007 to 2013 period, and further decreased to only 0.3 kg/m^3 during 2014 to 2017 (Fig. 14B). The SSCs at the SP2 and SP3 sites were still around 2.0 kg/m^3 in 2012 and dropped sharply since then (Fig. 14B). Therefore, it is believed that the low SSC directly contributes to the severe erosion and surficial sediment coarsening that occurred in the Nanhui Shoal and tidal flat, with the strongest erosion recorded at the delta front (Dai *et al.*, 2014; Luan *et al.*, 2016; Mei *et al.*, 2023). Luan *et al.* (2017) predicted that the shoals–channels system of the Changjiang Delta will suffer more severe erosion by 2030, especially when the terrigenous sediment input falls below 1.00 × 10^8 t/year. In the Yellow Delta and

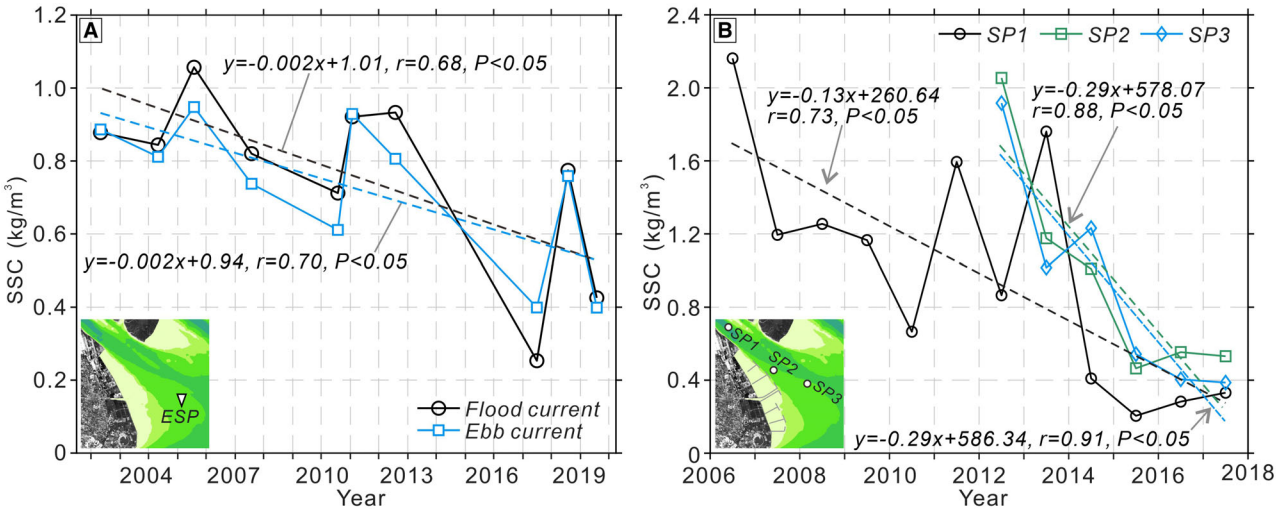

Fig. 14. Declines in annual suspended sediment concentrations (SSCs) of: (A) flood/ebb tidal currents around the East South Passage (ESP) station between 2003 and 2019; and (B) at three gauging stations (SP1 to SP3) along the South Passage between 2006 and 2017.

adjacent coasts, the reduced riverine sediment supply and stronger hydrodynamics have also triggered more sediment erosion, as a result, both surface and core sediments have coarsened since 1990 and recently intensified this trend (Liu *et al.*, 2022).

Transport pathways of suspended and bed sediments in mega-deltas also control sediment convergence–divergence patterns that lead to morphodynamic change (Fagherazzi & Overeem, 2007; Alonso *et al.*, 2021). *In situ* observations revealed that there is a 'dynamic equilibrium zone' of water and sediment transport between the Nanhui Shoal and Nanhui tidal flat, which is conducive to the convergence of bottom sediments towards intertidal flats and some subaqueous locations (Chen *et al.*, 2001; Yun, 2004). In deltas in the Gulf of Papua, sediment grain size in vibracores become finer upward, which indicates mesotidal forcing and enough sediment supply (Walsh & Nittrouer, 2004). The vertical variation pattern of sediment grain size in a core in the Nanhui tidal flat was the opposite, providing evidence for changes in the deltaic sedimentary system triggered by limited sediment availability and siltation-promoting engineering structures.

Specifically, both sediment-starved tidal currents and energetic waves can enhance sediment resuspension in offshore muddy substrates, resulting in more fine-grained sediments being taken away by littoral currents (Chen *et al.*, 2001; Xie *et al.*, 2017). In the northern part of the Nanhui Shoal, runoff with low SSC triggers erosion of coarser-grained material that is transported downstream by ebb tides (Li *et al.*, 2010). Moreover, a clockwise residual sediment current formed around the Nanhui Shoal (Fig. S2). Hence, from 2004 to 2021, the grain-size parameter contours changed from perpendicular to isobaths to parallel to isobaths (Fig. 4). Specifically, the direction of modelled bed shear stress increased in the northern Nanhui Shoal from 2004 to 2020, while decreasing in the southern areas (Fig. 10), which was well spatially correlated with the variations in sorting coefficient and skewness of sediment and bathymetric changes (Figs 5 and 8J; Appendix S2).

In addition, the impacts of human activities on the sediment source-to-sink pathways have increased in the Nanhui Shoal and tidal flat, Changjiang Delta. The Deep-water Navigation Channel and large siltation-promoting engineering structures have been constructed at the shore, while reservoirs were built in the watershed (Luan *et al.*, 2016). As a result, the North Branch has gradually changed into a flood-dominated tidal channel and offshore bed sediments have coarsened (Dai *et al.*, 2016b). Today, more fine-grained bed sediments are resuspended and partly deposited in some vegetated intertidal flats and within dykes of reclamation projects, thus further reducing sediment availability elsewhere (Yang *et al.*, 2005; Anthony *et al.*, 2014). In the mega-Changjiang Delta, the

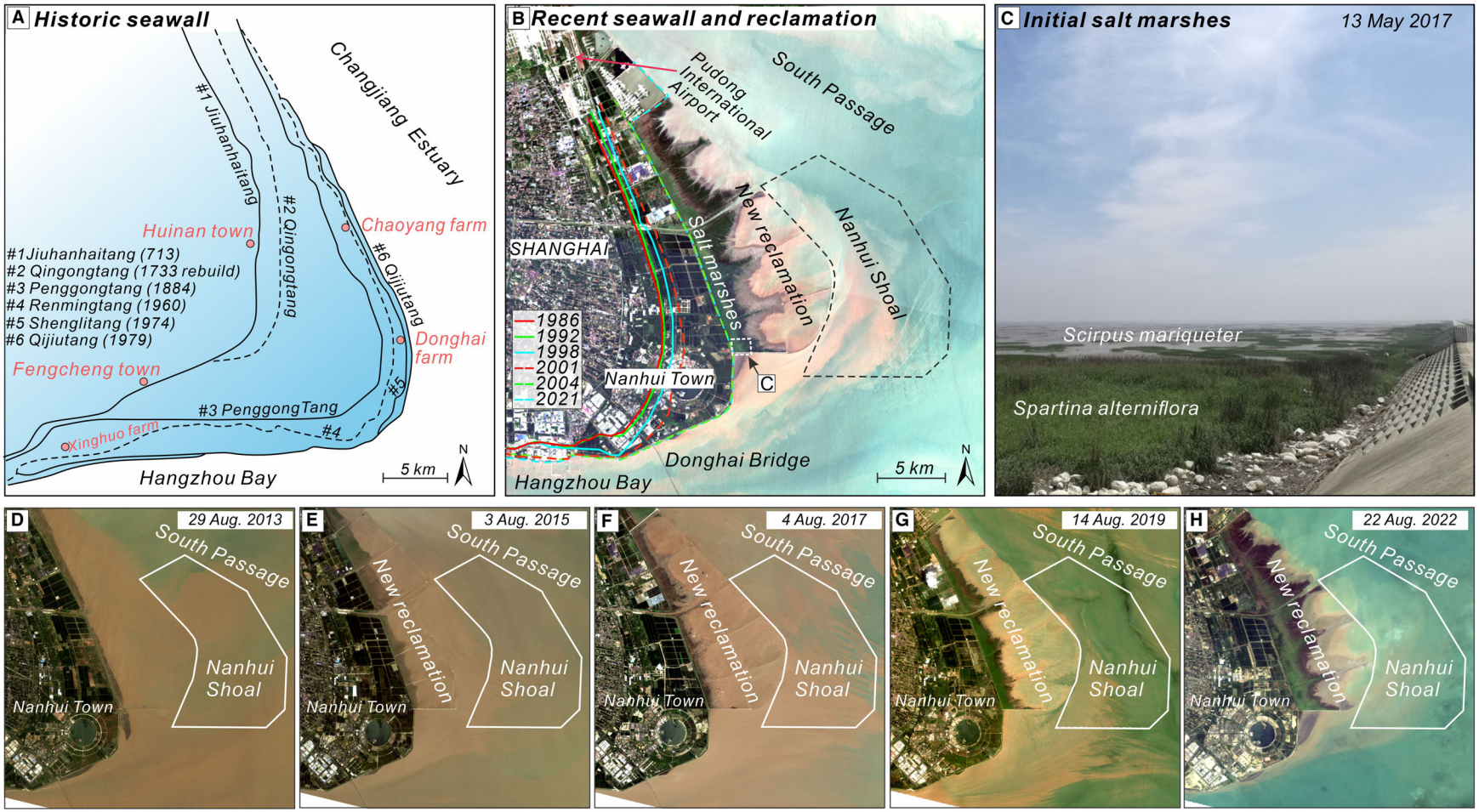

Fig. 15. (A) Historically constructed seawalls along the southern Changjiang Delta since 713 AD, and (B) recently implemented seawalls and reclamations in the Nanhui Shoal after 1986, the newest reclamation dykes were constructed in 2015. (C) Vegetation encroachment in the reclaimed areas in the east Nanhui tidal flat. (D) to (H) Time-series of Landsat images show changes in shorelines and land covers around the Nanhui Shoal and tidal flats from August 2013 to May 2022.

topographic slope in front of the engineering structure has abruptly increased, triggered by ebb tidal currents with very low SSC outflowing from the dyked area (most of the suspended sediment is deposited within the engineering structure). In the future, rising sea levels and storm waves will probably further reduce the sediment availability for tidal flats and shoals progradation in most mega-deltas, and alter the hydrodynamic conditions and sedimentary patterns (Schuerch *et al.*, 2014; Lentsch *et al.*, 2018).

Implications for tidal wetland sustainability

Interactions between runoff and tidal forcing are complex in mega-deltas; these processes determine sedimentary–geomorphic processes of tidal flats and wetlands (Anthony *et al.*, 2014; Hoitink *et al.*, 2017; Fagherazzi *et al.*, 2020). Before the TGD, the Nanhui Shoal was the fastest-depositing marginal shoal in the Changjiang Delta, with the progradation rate accelerating to 41 m/year between 1880 and 1960 (Chen *et al.*, 2001; Mao *et al.*, 2014). Historically, multi-stage reclamations and seawall construction have been carried out since 713 AD, to meet land needs and create wetlands (Fig. 15A). In the past 80 years, the subaerial area has increased by 20% in the Changjiang Delta (Yun, 2004). After the 1980s, construction of the new Nanhui Town on reclaimed tidal flats accelerated (Fig. 15B). This resulted in the demise of supratidal and intertidal zones, while the natural sediment transport and geomorphic equilibrium were disturbed (Wei *et al.*, 2017; Wang *et al.*, 2018; Mei *et al.*, 2023). The latest reclamations and siltation-promoting projects were implemented in the Nanhui tidal flats and Nanhui Shoal in 2014, after that the shoreline dramatically expanded seaward (Fig. 15B). Some eroded sediment from the subaqueous delta and South Passage deposited in dyked areas, leading to saltmarsh vegetation encroachment (Fig. 15C to H). The decline in sediment availability and enhanced bottom erosion can reduce the transfer of sediment from offshore to intertidal marshes, threatening their sustainability (Kennish, 2001; Schuerch *et al.*, 2014).

Furthermore, the impacts of sea-level rise superimposed on land subsidence are likely to amplify storm-wave hazards in deltas (Belliard *et al.*, 2016). These processes will primarily trigger intertidal/subtidal sediment resuspensions and pose significant challenges to the vulnerability of mega-deltas and their tidal wetlands (Bianchi & Allison, 2009; Karpytchev *et al.*, 2016; Wang *et al.*, 2020). Based on an analytical model and measured data, Nienhuis *et al.* (2018) proposed that tidally-driven sediments will be transported into present delta distributaries at a faster pace after reduced riverine runoff and sediment supply. In the mega-Changjiang Delta, some studies have shown that the heightened tidal forcing with high bed shear stress could resuspend more marine sediments and transport them landward, alleviating the strong erosion to a certain extent (Mei *et al.*, 2018b; Yang *et al.*, 2020; Leonardi *et al.*, 2021).

Li (2018) showed that the sorting coefficient of surficial sediments on the south side of the Nanhui Shoal is higher, but the skewness is lower (Fig. S3), which partly influenced the increase in sorting coefficient and the decrease of skewness from 2004 to 2020 (Fig. 5). Hence, this study demonstrates the specific shift process from a sedimentary point of view through high-precision sediment and bathymetric data. However, the impact of a reduction in fine-grained sediment fractions on sediment budgets and overall sediment availability needs further research.

CONCLUSIONS

The hydrodynamic and geomorphic processes of most mega-deltas are disrupted by human activities and sea-level rise. How large-scale deltaic flats and tidal wetlands respond to insufficient sediment supply and variations in marine forcing are not well-understood. Herein, sedimentary variations in the Nanhui tidal flat and Nanhui Shoal (the largest-growing shoal) in the Changjiang Delta were examined. The main conclusions are as follows:

1 The average sediment grain size deposited in the Nanhui Shoal overall coarsened from 18.5 μm in 2004 to 27.3 μm in 2021 (an increase of 48.0%) and was more poorly sorted. Sediment's average grain size deposited in the Nanhui intertidal flat increased since the 1990s and further coarsened to 40.2 μm (by 24.8%) during the post-TGD (Three Gorges Dam) period.

2 An increase in the Shannon's diversity index (SHDI) and a decrease in the contagion (CONTAG) index indicate that sediment patches around the Nanhui Shoal are more fragmented and less organized. In addition, the spatial patterns of sediment grain-size parameters have changed from crossing bathymetric isobaths to

being parallel to them, accompanied by erosion occurring in the northern subaqueous area.

3 Sustained sediment coarsening is attributed to severe delta erosion triggered by a decline in suspended sediment discharge (over 70%) after the TGD construction. The upstream coarsening of bed sediments also promoted the deposition of coarse sediments downstream.

4 Increasing diversion of runoff to the area, and an increase in the tidal level and strongest waves is hypothesized to have resulted in re-suspension and net export of fine-grained sediments in the mega-Changjiang Delta. These processes continue to impair sediment availability and the overall sustainability of the Nanhui Shoal and Nanhui tidal flats. This research is especially important because changes in tidal flats may induce degradations of deltaic tidal wetlands. the sedimentary variations that are occurring in the Changjiang Delta are likely to occur in other deltas around the world where sediment loading has been decreased substantially. Deltaic marshes and the ecological services they provide will be more severely challenged in the future.

ACKNOWLEDGEMENTS

We are grateful for the help in field work from Wen Wei, Wenhong Pang, Xiaoyan Zhou, Yun Chen, Zuming Huang, Jiangjie Yang, Runan Tang, Jiejun Luo, Xixin Liang, Ming Shi and Lingxiao Wang at East China Normal University. This study was supported financially by the Joint Key Funds of the National Natural Science Foundation of China (U2040202), the National Natural Science Foundation of China (42076174), Shanghai International Science and Technology Cooperation Fund Project (23230713800) and the Marine Science Program for Guangxi First-Class Discipline, Beibu Gulf University. Sergio Fagherazzi was partly funded by the USA National Science Foundation Award 2224608 (PIE LTER) and 1832221 (VCR LTER). We very sincerely acknowledge the constructive comments and careful suggestions from two anonymous reviewers and the Associate Editor Dr. J.P. Walsh.

CONFLICT OF INTEREST

The authors declare that they have no known competing financial interests or personal relationships that could have appeared to influence the work reported in this paper.

DATA AVAILABILITY STATEMENT

The water discharge and concentration, discharge and grain size of suspended sediment at Datong station were obtained from the Bureau of Hydrology, Changjiang River Water Resources Commission (http://www.cjh.com.cn/en/) and the Changjiang River Sediment Bulletins. Hydrodynamic data of the tidal levels, flow velocities–directions, and SSCs in the Changjiang Delta were measured by the Hydrology-Water Resources Survey Bureau of the Changjiang (Yangtze) Estuary, Changjiang Water Resources Committee, China. Landsat remote images were downloaded from the United States Geological Survey (https://glovis.usgs.gov/). Bathymetric data were acquired from the State Key Laboratory of Estuarine and Coastal Research, East China Normal University (http://english.sklec.ecnu.edu.cn/) and the Shanghai Institute of Geological Survey, China (https://www.sigs.cn/). More detailed information that supports this study is shown in the supplementary material and can be obtained from the corresponding author (Prof. Zhijun Dai, zjdai@sklec.ecnu.edu.cn) upon reasonable request.

REFERENCES

Alonso, A.C., **van Maren, D.S.**, **Elias, E.P.L.**, **Holthuijsen, S.J.** and **Wang, Z.B.** (2021) The contribution of sand and mud to infilling of tidal basins in response to a closure dam. *Mar. Geol.*, **439**, 106544.

Andersen, T.J., **Mikkelsen, O.A.**, **Møller, A.L.** and **Pejrup, M.** (2000) Deposition and mixing depths on some European intertidal mudflats based on ^{210}Pb and ^{137}Cs activities. *Cont. Shelf Res.*, **20**, 1569–1591.

Angamuthu, B., **Darby, S.E.** and **Nicholls, R.J.** (2018) Impacts of natural and human drivers on the multi-decadal morphological evolution of tidally-influenced deltas. *Proc. Math. Phys. Eng. Sci.*, **474**, 20180396.

Anthony, E.J., **Gardel, A.** and **Gratiot, N.** (2014) Fluvial sediment supply, mud banks, cheniers and the morphodynamics of the coast of South America between the Amazon and Orinoco river mouths. *Geol. Soc. Lond. Spec. Publ.*, **388**, 533–560.

Bainbridge, Z., **Lewis, S.**, **Bartley, R.**, **Fabricius, K.**, **Collier, C.**, **Waterhouse, J.**, **Garzon-Garcia, A.**, **Robson, B.**, **Burton, J.**, **Wenger, A.** and **Brodie, J.** (2018) Fine sediment and particulate organic matter: A review and case study on ridge-to-reef transport, transformations, fates, and impacts on marine ecosystems. *Mar. Pollut. Bull.*, **135**, 1205–1220.

Belliard, J.P., **Di Marco, N.**, **Carniello, L.** and **Toffolon, M.** (2016) Sediment and vegetation spatial dynamics facing sea-level rise in microtidal salt marshes: Insights from an ecogeomorphic model. *Adv. Water Resour.*, **93**, 249–264.

Besset, M., **Anthony, E.J.** and **Bouchette, F.** (2019) Multi-decadal variations in delta shorelines and their relationship to river sediment supply: An assessment and review. *Earth-Sci. Rev.*, **193**, 199–219.

Bianchi, T.S. and **Allison, M.A.** (2009) Large-river delta-front estuaries as natural "recorders" of global environmental change. *Proc. Natl. Acad. Sci.*, **106**, 8085–8092.

Blum, M.D. and **Roberts, H.H.** (2009) Drowning of the Mississippi Delta due to insufficient sediment supply and global sea-level rise. *Nat. Geosci.*, **2**, 488–491.

Bolla Pittaluga, M., **Tambroni, N.**, **Canestrelli, A.**, **Slingerland, R.**, **Lanzoni, S.** and **Seminara, G.** (2015) Where river and tide meet: The morphodynamic equilibrium of alluvial estuaries. *J. Geophys. Res. Earth*, **120**, 75–94.

Burdon, F.J., **McIntosh, A.R.** and **Harding, J.S.** (2013) Habitat loss drives threshold response of benthic invertebrate communities to deposited sediment in agricultural streams. *Ecol. Appl.*, **23**, 1036–1047.

Canestrelli, A., **Fagherazzi, S.**, **Defina, A.** and **Lanzoni, S.** (2010) Tidal hydrodynamics and erosional power in the Fly River delta, Papua New Guinea. *J. Geophys. Res. Earth*, **115**, F04033.

Canuel, E.A., **Spivak, A.C.**, **Waterson, E.J.** and **Emmett Duffy, J.** (2007) Biodiversity and food web structure influence short-term accumulation of sediment organic matter in an experimental seagrass system. *Limnol. Oceanogr.*, **52**, 590–602.

Carriquiry, J.D. and **Sánchez, A.** (1999) Sedimentation in the Colorado River delta and Upper Gulf of California after nearly a century of discharge loss. *Mar. Geol.*, **158**, 125–145.

Chambers, R.M., **Meyerson, L.A.** and **Saltonstall, K.** (1999) Expansion of Phragmites australis into tidal wetlands of North America. *Aquat Botany*, **64**, 261–273.

Changjiang Water Resources Commission (CWRC) (2020) *Changjiang River Sediment Bulletin*. Changjiang Press, Wuhan. (in Chinese).

Chen, J.Y., **Shen, H.T.** and **Yun, C.X.** (1988) *Hydrodynamics and Geomorphic Evolution in the Yangtze (Changjiang) Estuary*. Shanghai Science and Technology Press, Shanghai. (in Chinese).

Chen, J.Y., **Li, D.J.**, **Chen, B.L.**, **Hu, F.X.**, **Zhu, H.F.** and **Liu, C.Z.** (1999) The processes of dynamic sedimentation in the Changjiang Estuary. *J Sea Res.*, **41**, 129–140.

Chen, J.Y., **Chen, S.L.**, **Ding, P.X.** and **Yang, S.L.** (2001) Sediment transport along the Nanhui submerged spit of the Yangtze Estuary. *Res. Environ. Yangtze Basin*, **10**, 166–172 (in Chinese with English Abstract).

Chen, Y., **Dong, J.W.**, **Xiao, X.M.**, **Zhang, M.**, **Tian, B.**, **Zhou, Y.X.**, **Li, B.** and **Ma, Z.J.** (2016) Land claim and loss of tidal flats in the Yangtze Estuary. *Sci. Rep.*, **6**, 1–10.

Cui, L.F., **Ge, Z.M.**, **Yuan, L.** and **Zhang, L.Q.** (2015) Vulnerability assessment of the coastal wetlands in the Yangtze Estuary, China to sea-level rise. *Estuar. Coast. Shelf Sci.*, **156**, 42–51.

Dai, Z.J. and **Liu, J.T.** (2013) Impacts of large dams on downstream fluvial sedimentation: An example of the Three Gorges Dam (TGD) on the Changjiang (Yangtze River). *J. Hydrol.*, **480**, 10–18.

Dai, Z.J., **Chen, J.Y.** and **Lu, H.T.** (2008) Analysis on the spatial on the spatial distribution of deposition fields between the east bank and the south bank, in the Changjiang River estuary. *Transac. Oceanol. Limnol.*, **2**, 46–52 (in Chinese with English abstract).

Dai, Z.J., **Liu, J.T.**, **Wei, W.** and **Chen, J.Y.** (2014) Detection of the three Gorges Dam influence on the Changjiang (Yangtze River) submerged delta. *Sci. Rep.*, **4**, 1–7.

Dai, Z.J., **Liu, J.T.** and **Wen, W.** (2015) Morphological evolution of the south passage in the Changjiang (Yangtze River) estuary, China. *Quat. Int.*, **380**, 314–326.

Dai, Z.J., **Fagherazzi, S.**, **Mei, X.F.** and **Gao, J.J.** (2016a) Decline in suspended sediment concentration delivered by the Changjiang (Yangtze) River into the East China Sea between 1956 and 2013. *Geomorphology*, **268**, 123–132.

Dai, Z.J., **Fagherazzi, S.**, **Mei, X.F.**, **Chen, J.Y.** and **Meng, Y.** (2016b) Linking the infilling of the North Branch in the Changjiang (Yangtze) estuary to anthropogenic activities from 1958 to 2013. *Mar. Geol.*, **379**, 1–12.

Dai, Z.J., **Mei, X.F.**, **Darby, S.E.**, **Lou, Y.Y.** and **Li, W.H.** (2018) Fluvial sediment transfer in the Changjiang (Yangtze) river-estuary depositional system. *J. Hydrol.*, **566**, 719–734.

Deltares (2014) *User Manual Delft3D-Flow: Simulation of Multi-dimensional Hydrodynamic Flows and Transport Phenomena, Including Sediments. Version 3.15*. Deltares, Delft.

Dethier, E.N., **Renshaw, C.E.** and **Magilligan, F.J.** (2022) Rapid changes to global river suspended sediment flux by humans. *Science*, **376**, 1447–1452.

Donatelli, C., **Zhang, X.H.**, **Ganju, N.K.**, **Aretxabaleta, A.L.**, **Fagherazzi, S.** and **Leonardi, N.** (2020) A nonlinear relationship between marsh size and sediment trapping capacity compromises salt marshes' stability. *Geology*, **48**, 966–970.

Dong, S.C., **Samsonov, S.**, **Yin, H.W.**, **Ye, S.J.** and **Cao, Y.R.** (2014) Time-series analysis of subsidence associated with rapid urbanization in Shanghai, China measured with SBAS InSAR method. *Environ. Earth Sci.*, **72**, 677–691.

Edmonds, D.A. and **Slingerland, R.L.** (2010) Significant effect of sediment cohesion on delta morphology. *Nat. Geosci.*, **3**, 105–109.

Fagherazzi, S. and **Overeem, I.** (2007) Models of deltaic and inner continental shelf landform evolution. *Annu. Rev. Earth Planet. Sci.*, **35**, 685–715.

Fagherazzi, S., **Edmonds, D.A.**, **Nardin, W.**, **Leonardi, N.**, **Canestrelli, A.**, **Falcini, F.**, **Jerolmack, D.J.**, **Mariotti, G.**, **Rowland, J.C.** and **Slingerland, R.L.** (2015) Dynamics of river mouth deposits. *Rev. Geophys.*, **53**, 642–672.

Fagherazzi, S., **Mariotti, G.**, **Leonardi, N.**, **Canestrelli, A.**, **Nardin, W.** and **Kearney, W.S.** (2020) Salt marsh dynamics in a period of accelerated sea level rise. *J. Geophys. Res. Earth*, **125**, e2019JF005200.

Fan, D.D., **Wu, Y.J.**, **Zhang, Y.**, **Burr, G.**, **Huo, M.** and **Li, J.** (2017) South Flank of the Yangtze Delta: Past, present, and future. *Mar. Geol.*, **392**, 78–93.

Fitzgerald, D.M., **Kulp, M.**, **Penland, S.**, **Flocks, J.** and **Kindinger, J.** (2004) Morphologic and stratigraphic evolution of muddy ebb-tidal deltas along a subsiding coast: Barataria Bay, Mississippi River Delta. *Sedimentology*, **51**, 1157–1178.

Folk, R.L. and **Ward, W.C.** (1957) Brazos River bar: a study in the significance of grain size parameters. *J. Sediment. Res.*, **27**, 3–26.

Frihy, O.E. (2003) The Nile delta-Alexandria coast: vulnerability to sea-level rise, consequences and adaptation. *Mitig. Adapt. Strat. Glob. Chang.*, **8**, 115–138.

Ganju, N.K., **Kirwan, M.L.**, **Dickhudt, P.J.**, **Guntenspergen, G.R.**, **Cahoon, D.R.** and **Kroeger, K.D.** (2015) Sediment transport-based metrics of wetland stability. *Geophys. Res. Lett.*, **42**, 7992–8000.

Ge, Z.M., **Cao, H.B.**, **Cui, L.F.**, **Zhao, B.** and **Zhang, L.Q.** (2015) Future vegetation patterns and primary production in the coastal wetlands of East China under sea level rise, sediment reduction, and saltwater intrusion. *J. Geophys. Res. Biogeo.*, **120**, 1923–1940.

Giosan, L., **Constantinescu, S.**, **Clift, P.D.**, **Tabrez, A.R.**, **Danish, M.** and **Inam, A.** (2006) Recent morphodynamics

of the Indus delta shore and shelf. *Cont. Shelf Res.*, **26**, 1668–1684.

Green, M.O. and **Coco, G.** (2014) Review of wave-driven sediment resuspension and transport in estuaries. *Rev. Geophys.*, **52**, 77–117.

Guo, X.J., **Fan, D.D.**, **Zheng, S.W.**, **Wang, H.M.**, **Zhao, B.C.** and **Qin, C.J.** (2021) Revisited sediment budget with latest bathymetric data in the highly altered Yangtze (Changjiang) Estuary. *Geomorphology*, **391**, 107873.

Harley, M.D., **Turner, I.L.**, **Kinsela, M.A.**, **Middleton, J.H.**, **Mumford, P.J.**, **Splinter, K.D.**, **Phillips, M.S.**, **Simmons, J.A.**, **Hanslow, D.J.** and **Short, A.D.** (2017) Extreme coastal erosion enhanced by anomalous extratropical storm wave direction. *Sci. Rep.*, **7**, 1–9.

Hoitink, A.J.F., **Wang, Z.B.**, **Vermeulen, B.**, **Huismans, Y.** and **Kästner, K.** (2017) Tidal controls on river delta morphology. *Nat. Geosci.*, **10**, 637–645.

Hong, S.K., **Koh, C.H.**, **Harris, R.R.**, **Kim, J.E.**, **Lee, J.S.** and **Ihm, B.S.** (2010) Land use in Korean tidal wetlands: impacts and management strategies. *Environ. Manag.*, **45**, 1014–1026.

Hori, K., **Saito, Y.**, **Zhao, Q.H.**, **Cheng, X.R.**, **Wang, P.X.**, **Sato, Y.** and **Li, C.X.** (2001) Sedimentary facies and Holocene progradation rates of the Changjiang (Yangtze) delta, China. *Geomorphology*, **41**, 233–248.

Hori, K., **Saito, Y.**, **Zhao, Q.H.** and **Wang, P.X.** (2002) Architecture and evolution of the tide-dominated Changjiang (Yangtze) River delta, China. *Sediment. Geol.*, **146**, 249–264.

Imperato, D.P., **Sexton, W.J.** and **Hayes, M.O.** (1988) Stratigraphy and sediment characteristics of a mesotidal ebb-tidal delta, North Edisto Inlet, South Carolina. *J. Sediment. Res.*, **58**, 950–958.

Karpytchev, M., **Ballu, V.**, **Krien, Y.**, **Becker, M.**, **Goodbred, S.**, **Spada, G.**, **Calmant, S.**, **Shum, C.K.**, **Kelleway, J.J.**, **Saintilan, N.**, **Macreadie, P.I.**, **Skilbeck, C.G.**, **Zawadzki, A.** and **Ralph, P.J.** (2016) Seventy years of continuous encroachment substantially increases 'blue carbon' capacity as mangroves replace intertidal salt marshes. *Glob. Chang. Biol.*, **22**, 1097–1109.

Kästner, K., **Hoitink, A.J.F.**, **Vermeulen, B.**, **Geertsema, T.J.** and **Ningsih, N.S.** (2017) Distributary channels in the fluvial to tidal transition zone. *J. Geophys. Res. Earth*, **122**, 696–710.

Kennish, M.J. (2001) Coastal salt marsh systems in the US: a review of anthropogenic impacts. *J. Coast. Res.*, **17**, 731–748.

Kirwan, M.L. and **Megonigal, J.P.** (2013) Tidal wetland stability in the face of human impacts and sea-level rise. *Nature*, **504**, 53–60.

Kirwan, M.L., **Walters, D.C.**, **Reay, W.G.** and **Carr, J.A.** (2016) Sea level driven marsh expansion in a coupled model of marsh erosion and migration. *Geophys. Res. Lett.*, **43**, 4366–4373.

Kondolf, G.M., **Schmitt, R.J.P.**, **Carling, P.A.**, **Goichot, M.**, **Keskinen, M.**, **Arias, M.E.**, **Bizzi, S.**, **Castelletti, A.**, **Cochrane, T.A.**, **Darby, S.E.**, **Kummu, M.**, **Minderhoud, P.S.J.**, **Nguyen, D.**, **Nguyen, H.T.**, **Nguyen, N.T.**, **Oeurng, C.**, **Opperman, J.**, **Rubin, Z.**, **San, D.C.**, **Schmeier, S.** and **Wild, T.** (2022) Save the Mekong Delta from drowning. *Science*, **376**, 583–585.

Lee, J., **Kwon, B.O.**, **Kim, B.**, **Noh, J.**, **Hwang, K.**, **Ryu, J.**, **Park, J.**, **Hong, S.** and **Khim, J.S.** (2019) Natural and anthropogenic signatures on sedimentary organic matters across varying intertidal habitats in the Korean waters. *Environ. Int.*, **133**, 105166.

Lentsch, N., **Finotello, A.** and **Paola, C.** (2018) Reduction of deltaic channel mobility by tidal action under rising relative sea level. *Geology*, **46**, 599–602.

Leonardi, N., **Mei, X.F.**, **Carnacina, I.** and **Dai, Z.J.** (2021) Marine sediment sustains the accretion of a mixed fluvial-tidal delta. *Mar. Geol.*, **438**, 106520.

Leuven, J.R.F.W., **van Keulen, D.**, **Nienhuis, J.H.**, **Canestrelli, A.** and **Hoitink, A.J.F.** (2021) Large-scale scour in response to tidal dominance in estuaries. *J. Geophys. Res. Earth*, **126**, e2020JF006048.

Li, J.F. (1991) The rule of sediment transport on the Nanhui tidal flat in the Changjiang Estuary. *Acta Oceanologica Sinica*, **1**, 117–127.

Li, Y.M. (2018) *Studies on Sediment Characteristics and the Influencing Factors in the Yangtze Estuary Riverbed during the Recent 30 Years*. Doctoral dissertation. East China Normal University, Shanghai. (in Chinese with English Abstract).

Li, J.F., **Dai, Z.J.**, **Liu, X.C.**, **Zhao, J.C.** and **Feng, L.X.** (2010) Research on the movement of water and suspended sediment and sedimentation in Nanhui spit of the Yangtze Estuary before and after the construction of the reclamation projects on the tidal flat. *J. Sediment. Res.*, **3**, 31–37 (in Chinese with English Abstract).

Liu, L., **Wang, H.J.**, **Yang, Z.S.**, **Fan, Y.Y.**, **Wu, X.**, **Hu, L.M.** and **Bi, N.S.** (2022) Coarsening of sediments from the Huanghe (Yellow River) delta-coast and its environmental implications. *Geomorphology*, **401**, 108105.

Luan, H.L., **Ding, P.X.**, **Wang, Z.B.**, **Ge, J.Z.** and **Yang, S.L.** (2016) Decadal morphological evolution of the Yangtze Estuary in response to river input changes and estuarine engineering projects. *Geomorphology*, **265**, 12–23.

Luan, H.L., **Ding, P.X.**, **Wang, Z.B.** and **Ge, J.Z.** (2017) Process-based morphodynamic modeling of the Yangtze Estuary at a decadal timescale: Controls on estuarine evolution and future trends. *Geomorphology*, **290**, 347–364.

Luo, J.J., **Dai, Z.J.**, **Wang, J.**, **Lou, Y.Y.**, **Zhou, X.Y.** and **Tang, R.N.** (2023) Effects of human-induced riverine sediment transfer on deposition-erosion in the South Passage of the Changjiang (Yangtze) delta. *J. Hydrol.*, **129714**, 129714.

Maloney, J.M., **Bentley, S.J.**, **Xu, K.**, **Obelcz, J.**, **Georgiou, I.Y.** and **Miner, M.D.** (2018) Mississippi River subaqueous delta is entering a stage of retrogradation. *Mar. Geol.*, **400**, 12–23.

Mao, Z.C. (1987) The role of wave action in scouring and siltation processes of east Nanhui tidal flat. *Transac. Oceanol. Limnol.*, **4**, 21–29.

Mao, Z.C., **Yu, Z.Y.** and **Xu, H.G.** (2014) *Study on Tidal Flats in Shanghai*. East China Normal University Press, Shanghai. (in Chinese).

Marriner, N., **Flaux, C.**, **Morhange, C.** and **Kaniewski, D.** (2012) Nile Delta's sinking past: Quantifiable links with Holocene compaction and climate-driven changes in sediment supply? *Geology*, **40**, 1083–1086.

Mei, X., **Du, J.Z.**, **Dai, Z.J.**, **Du, J.**, **Gao, J.J.** and **Wang, J.** (2018a) Decadal Sedimentation in China's Largest Freshwater Lake, Poyang Lake. *Geochem. Geophys. Geosyst.*, **19**, 2384–2396.

Mei, X.F., **Dai, Z.J.**, **Wei, W.**, **Li, W.H.**, **Wang, J.** and **Sheng, H.** (2018b) Secular bathymetric variations of the North Channel in the Changjiang (Yangtze) Estuary, China, 1880–2013: Causes and effects. *Geomorphology*, **303**, 30–40.

Mei, X.F., **Dai, Z.J.**, **Darby, S.E.**, **Zhang, M.**, **Cai, H.Y.**, **Wang, J.** and **Wei, W.** (2021) Landward shifts of the maximum accretion zone in the tidal reach of the Changjiang estuary following construction of the Three Gorges Dam. *J. Hydrol.*, **592**, 125789.

Mei, X.F., **Leonardi, N.**, **Dai, J.X.** and **Wang, J.** (2023) Cellular automata to understand the prograding limit of deltaic tidal flat. *Eng. App. Comput. Fluid Mech.*, **17**, 2234038.

Michels, K.H., **Kudrass, H.R.**, **Hübscher, C.**, **Suckow, A.** and **Wiedicke, M.** (1998) The submarine delta of the Ganges-Brahmaputra: cyclone-dominated sedimentation patterns. *Mar. Geol.*, **149**, 133–154.

Milliman, J.D. and **Meade, R.H.** (1983) World-wide delivery of river sediment to the oceans. *J. Geol.*, **91**, 1–21.

Möller, I., **Kudella, M.**, **Rupprecht, F.**, **Spencer, T.**, **Paul, M.**, **Van Wesenbeeck, B.K.**, **Wolters, G.**, **Jensen, K.**, **Bouma, T.J.**, **Miranda-Lange, M.** and **Schimmels, S.** (2014) Wave attenuation over coastal salt marshes under storm surge conditions. *Nat. Geosci.*, **7**, 727–731.

Murray, N.J., **Phinn, S.R.**, **DeWitt, M.**, **Ferrari, R.**, **Johnston, R.**, **Lyons, M.B.**, **Clinton, N.**, **Thau, D.** and **Fuller, R.A.** (2019) The global distribution and trajectory of tidal flats. *Nature*, **565**, 222–225.

Murray, N.J., **Worthington, T.A.**, **Bunting, P.**, **Duce, S.**, **Hagger, V.**, **Lovelock, C.E.**, **Lucas, R.**, **Saunders, M.I.**, **Sheaves, M.**, **Spalding, M.**, **Waltham, N.J.** and **Lyons, M.B.** (2022) High-resolution mapping of losses and gains of Earth's tidal wetlands. *Science*, **376**, 744–749.

Nienhuis, J.H., **Hoitink, A.J.F.** and **Törnqvist, T.E.** (2018) Future change to tide-influenced deltas. *Geophys. Res. Lett.*, **45**, 3499–3507.

Nilsson, C., **Reidy, C.A.**, **Dynesius, M.** and **Revenga, C.** (2005) Fragmentation and flow regulation of the world's large river systems. *Science*, **308**, 405–408.

Orton, G.J. and **Reading, H.G.** (1993) Variability of deltaic processes in terms of sediment supply, with particular emphasis on grain size. *Sedimentology*, **40**, 475–512.

Paola, C., **Twilley, R.R.**, **Edmonds, D.A.**, **Kim, W.**, **Mohrig, D.**, **Parker, G.**, **Viparelli, E.** and **Voller, V.R.** (2011) Natural processes in delta restoration: Application to the Mississippi Delta. *Ann. Rev. Mar. Sci.*, **3**, 67–91.

Plink-Björklund, P. (2008) Wave-to-tide facies change in a Campanian shoreline complex, Chimney Rock Tongue, Wyoming-Utah, USA. In: *Recent Advances in Models of Shallow-Marine Stratigraphy* (Eds Hampson, G.J., Steel, R.J., Burgess, P.M. and Dalrymple, B.W.), *SEPM Spec. Publ*, **90**, 265–291.

Plink-Björklund, P. (2012) Effects of tides on deltaic deposition: Causes and responses. *Sediment. Geol.*, **279**, 107–133.

Qi, Z.F., **Ye, X.Y.**, **Zhang, H.** and **Yu, Z.L.** (2014) Land fragmentation and variation of ecosystem services in the context of rapid urbanization: The case of Taizhou city, China. *Stochastic Environ. Res. Risk Assess.*, **28**, 843–855.

Ridderinkhof, H., **van der Ham, R.** and **van der Lee, W.** (2000) Temporal variations in concentration and transport of suspended sediments in a channel-flat system in the Ems-Dollard estuary. *Cont. Shelf Res.*, **20**, 1479–1493.

Rodriguez, A.B., **McKee, B.A.**, **Miller, C.B.**, **Bost, M.C.** and **Atencio, A.N.** (2020) Coastal sedimentation across North America doubled in the 20th century despite river dams. *Nat. Commun.*, **11**, 1–9.

Rogers, K., **Kelleway, J.J.**, **Saintilan, N.**, **Megonigal, J.P.**, **Adams, J.B.**, **Holmquist, J.R.**, **Lu, M.**, **Schile-Beers, L.**, **Zawadzki, A.**, **Mazumder, D.** and **Woodroffe, C.D.** (2019) Wetland carbon storage controlled by millennial-scale variation in relative sea-level rise. *Nature*, **567**, 91–95.

Ryżak, M. and **Bieganowski, A.** (2011) Methodological aspects of determining soil particle-size distribution using the laser diffraction method. *J. Plant Nutr. Soil Sci.*, **174**, 624–633.

Schile, L.M., **Callaway, J.C.**, **Morris, J.T.**, **Stralberg, D.**, **Parker, V.T.** and **Kelly, M.** (2014) Modeling tidal marsh distribution with sea-level rise: evaluating the role of vegetation, sediment, and upland habitat in marsh resiliency. *PLoS One*, **9**, e88760.

Schuerch, M., **Dolch, T.**, **Reise, K.** and **Vafeidis, A.T.** (2014) Unravelling interactions between salt marsh evolution and sedimentary processes in the Wadden Sea (southeastern North Sea). *Prog. Phys. Geogr.*, **38**, 691–715.

Schuerch, M., **Spencer, T.**, **Temmerman, S.**, **Kirwan, M.L.**, **Wolff, C.**, **Lincke, D.**, **McOwen, C.J.**, **Pickering, M.D.**, **Reef, R.**, **Vafeidis, A.T.**, **Hinkel, J.**, **Nicholls, R.J.** and **Brown, S.** (2018) Future response of global coastal wetlands to sea-level rise. *Nature*, **561**, 231–234.

Scully, M.E. and **Friedrichs, C.T.** (2007) Sediment pumping by tidal asymmetry in a partially mixed estuary. *J. Geophys. Res. Oceans*, **112**, C07028.

Shi, Z.H., **Ai, L.**, **Li, X.**, **Huang, X.D.**, **Wu, G.L.** and **Liao, W.** (2013) Partial least-squares regression for linking land-cover patterns to soil erosion and sediment yield in watersheds. *J. Hydrol.*, **498**, 165–176.

Sibson, R. (1981) A brief description of natural neighbor interpolation. In: *Interpreting Multivariate Data* (Ed Barnett, V.), pp. 21–36. John Wiley & Sons, New York, NY.

Sperazza, M., **Moore, J.N.** and **Hendrix, M.S.** (2004) High-resolution particle size analysis of naturally occurring very fine-grained sediment through laser diffractometry. *J. Sediment. Res.*, **74**, 736–743.

Syvitski, J.P., **Vörösmarty, C.J.**, **Kettner, A.J.** and **Green, P.** (2005) Impact of humans on the flux of terrestrial sediment to the global coastal ocean. *Science*, **308**, 376–380.

Syvitski, J.P., **Kettner, A.J.**, **Overeem, I.**, **Hutton, E.W.**, **Hannon, M.T.**, **Brakenridge, G.R.**, **Day, J.**, **Vörösmarty, C.**, **Saito, Y.**, **Giosan, L.** and **Nicholls, R.J.** (2009) Sinking deltas due to human activities. *Nat. Geosci.*, **2**, 681–686.

Tamura, T., **Saito, Y.**, **Nguyen, V.L.**, **Ta, T.O.**, **Bateman, M.D.**, **Matsumoto, D.** and **Yamashita, S.** (2012) Origin and evolution of interdistributary delta plains; insights from Mekong River delta. *Geology*, **40**, 303–306.

Tessler, Z.D., **Vörösmarty, C.J.**, **Grossberg, M.**, **Gladkova, I.**, **Aizenman, H.**, **Syvitski, J.P.** and **Foufoula-Georgiou, E.** (2015) Profiling risk and sustainability in coastal deltas of the world. *Science*, **349**, 638–643.

Thorne, K., **MacDonald, G.**, **Guntenspergen, G.**, **Ambrose, R.**, **Buffington, K.**, **Dugger, B.**, **Freeman, C.**, **Janousek, C.**, **Brown, L.**, **Rosencranz, J.**, **Holmquist, J.**, **Smol, J.**, **Hargan, K.** and **Takekawa, J.** (2018) US Pacific coastal wetland resilience and vulnerability to sea-level rise. Science. *Advances*, **4**, eaao3270.

Ulses, C., **Estournel, C.**, **De Madron, X.D.** and **Palanques, A.** (2008) Suspended sediment transport in the Gulf of Lions (NW Mediterranean): Impact of extreme storms and floods. *Cont. Shelf Res.*, **28**, 2048–2070.

Unverricht, D., **Szczuciński, W.**, **Stattegger, K.**, **Jagodziński, R.**, **Le, X.T.** and **Kwong, L.L.W.** (2013) Modern sedimentation and morphology of the subaqueous Mekong Delta, Southern Vietnam. *Global Planet. Change*, **110**, 223–235.

Uuemaa, E., **Roosaare, J.** and **Mander, Ü.** (2007) Landscape metrics as indicators of river water quality at catchment scale. *Hydrol. Res.*, **38**, 125–138.

Uuemaa, E., **Roosaare, J.**, **Kanal, A.** and **Mander, Ü.** (2008) Spatial correlograms of soil cover as an indicator of landscape heterogeneity. *Ecol. Indic.*, **8**, 783–794.

Walsh, J.P. and **Nittrouer, C.A.** (2004) Mangrove-bank sedimentation in a mesotidal environment with large sediment supply, Gulf of Papua. *Mar. Geol.*, **208**, 225–248.
Walsh, J.P. and **Nittrouer, C.A.** (2009) Understanding fine-grained river-sediment dispersal on continental margins. *Mar. Geol.*, **263**, 34–45.
Walsh, J.P., **Corbett, D.R.**, **Kiker, J.M.**, **Orpin, A.R.**, **Hale, R.P.** and **Ogston, A.S.** (2014) Spatial and temporal variability in sediment deposition and seabed character on the Waipaoa River margin, New Zealand. *Cont. Shelf Res.*, **86**, 85–102.
Wang, H.J., **Wu, X.**, **Bi, N.S.**, **Li, S.**, **Yuan, P.**, **Wang, A.M.**, **Syvitski, J.P.M.**, **Saitoe, Y.**, **Yang, Z.S.**, **Liu, S.M.** and **Nittrouer, J.** (2017) Impacts of the dam-orientated water-sediment regulation scheme on the lower reaches and delta of the Yellow River (Huanghe): A review. *Global Planet. Change*, **157**, 93–113.
Wang, J., **Dai, Z.J.**, **Wei, W.**, **Ge, Z.P.**, **Pang, W.H.**, **Ma, B.B.**, **Mei, X.F.** and **Yu, Y.W.** (2018) LiDAR-based recent morphodynamic study of south Nanhui tidal flat, Changjiang Estuary. *Oceanologia et Limnologia Sinica*, **49**, 756–768. (in Chinese with English Abstract).
Wang, J., **Dai, Z.J.**, **Mei, X.F.** and **Fagherazzi, S.** (2020) Tropical cyclones significantly alleviate mega-deltaic erosion induced by high riverine flow. *Geophys. Res. Lett.*, **47**, e2020GL089065.
Wang, J., **Dai, Z.**, **Fagherazzi, S.** and **Long, C.** (2022a) A novel approach to discriminate sedimentary characteristics of deltaic tidal flats with terrestrial laser scanner: Results from a case study. *Sedimentology*, **69**, 1626–1648.
Wang, J., **Dai, Z.J.**, **Fagherazzi, S.**, **Zhang, X.H.** and **Liu, X.Q.** (2022b) Hydro-morphodynamics triggered by extreme riverine floods in a mega fluvial-tidal delta. *Sci. Total Environ.*, **809**, 152076.
Wei, W., **Dai, Z.J.**, **Mei, X.F.**, **Liu, J.P.**, **Gao, S.** and **Li, S.S.** (2017) Shoal morphodynamics of the Changjiang (Yangtze) estuary: Influences from river damming, estuarine hydraulic engineering and reclamation projects. *Mar. Geol.*, **386**, 32–43.
Wei, W., **Dai, Z.J.**, **Mei, X.F.**, **Gao, S.** and **Liu, J.P.** (2019) Multi-decadal morpho-sedimentary dynamics of the largest Changjiang estuarine marginal shoal: Causes and implications. *Land Degrad. Develop.*, **30**, 2048–2063.
Widdows, J. and **Brinsley, M.** (2002) Impact of biotic and abiotic processes on sediment dynamics and the consequences to the structure and functioning of the intertidal zone. *J. Sea Res.*, **48**, 143–156.
Wolinsky, M.A., **Edmonds, D.A.**, **Martin, J.** and **Paola, C.** (2010) Delta allometry: Growth laws for river deltas. *Geophys. Res. Lett.*, **37**, 592.
Xie, D.F., **Pan, C.H.**, **Wu, X.G.**, **Gao, S.** and **Wang, Z.B.** (2017) The variations of sediment transport patterns in the outer Changjiang Estuary and Hangzhou Bay over the last 30 years. *J. Geophys. Res. Oceans*, **122**, 2999–3020.
Yamashita, S., **Nakajo, T.**, **Naruse, H.** and **Sato, T.** (2009) The three-dimensional distribution of sedimentary facies and characteristics of sediment grain-size distribution in a sandy tidal flat along the Kushida River estuary, Ise Bay, central Japan. *Sediment. Geol.*, **215**, 70–82.
Yan, H., **Dai, Z.J.**, **Li, J.F.**, **Zhao, J.C.** and **Zhang, X.L.** (2009) Distribution of Surficial Tidal Flat Sediments in the Yangtze Estuary. *Acta Geographica Sinica*, **64**, 629–637. (in Chinese with English Abstract).
Yang, S.L., **Ding, P.X.** and **Zhao, Q.Y.** (2002) Morphodynamic response of a large river mouth to typhoons. *Ocean Eng.*, **3**, 69–75. (in Chinese with English Abstract).
Yang, S.L., **Zhang, J.**, **Zhu, J.**, **Smith, J.P.**, **Dai, S.B.**, **Gao, A.** and **Li, P.** (2005) Impact of dams on Yangtze River sediment supply to the sea and delta intertidal wetland response. *J. Geophys. Res. Earth*, **110**, 271.
Yang, S.L., **Milliman, J.D.**, **Xu, K.H.**, **Deng, B.**, **Zhang, X.Y.** and **Luo, X.X.** (2014) Downstream sedimentary and geomorphic impacts of the Three Gorges Dam on the Yangtze River. *Earth-Sci. Rev.*, **138**, 469–486.
Yang, S.L., **Luo, X.**, **Temmerman, S.**, **Kirwan, M.**, **Bouma, T.**, **Xu, K.**, **Zhang, S.S.**, **Fan, J.Q.**, **Shi, B.W.**, **Yang, H.F.**, **Wang, Y.P.**, **Shi, X.F.** and **Gao, S.** (2020) Role of delta-front erosion in sustaining salt marshes under sea-level rise and fluvial sediment decline. *Limnol. Oceanogr.*, **65**, 1990–2009.
Yarnell, S.M., **Mount, J.F.** and **Larsen, E.W.** (2006) The influence of relative sediment supply on riverine habitat heterogeneity. *Geomorphology*, **80**, 310–324.
Yun, C.X. (2004) *Basic Law of the Recent Evolution of the Changjiang Estuary*. China Ocean Press, Beijing. (in Chinese).
Zhang, X.H., **Fagherazzi, S.**, **Leonardi, N.** and **Li, J.F.** (2018) A positive feedback between sediment deposition and tidal prism may affect the morphodynamic evolution of tidal deltas. *J. Geophys. Res. Earth*, **123**, 2767–2783.
Zhou, X.Y., **Dai, Z.J.** and **Mei, X.F.** (2020) The multi-decadal morphodynamic changes of the mouth bar in a mixed fluvial-tidal estuarine channel. *Mar. Geol.*, **429**, 106311.
Zhu, L., **He, Q.**, **Shen, J.** and **Wang, Y.Y.** (2016) The influence of human activities on morphodynamics and alteration of sediment source and sink in the Changjiang Estuary. *Geomorphology*, **273**, 52–62.

Manuscript received 28 May 2023; revision accepted 8 November 2023

Supporting Information

Additional information may be found in the online version of this article:

Appendix S1. Sediment grain-size measurements.

Appendix S2. Spatial patterns of sedimentary variations.

Fig. S1. Changes in the monthly (A) average and (B) maximum grain size of riverine suspended sediments at upstream Datong station.

Fig. S2. (A) Tidal current roses at multiple hydrodynamic gauging sites in the southern Changjiang Delta, showing the 0 m, −2 m and −5 m isobaths, and (B) the spatial patterns of net sediment transport directions around the Nanhui Shoal (Li *et al.*, 2010).

Fig. S3. Spatial patterns of (A) sorting coefficient and (B) skewness of the subaqueous sediments in the southern Changjiang Delta in 2015 (Li *et al.*, 2018).

Table S1. Proportions of different grades of average grain size, sorting coefficient and skewness of sediments collected in the Nanhui Shoal.